

PREPARATION AND OPERATIONS OF THE MISSION PERFORMANCE
CENTRE (MPC) FOR THE COPERNICUS SENTINEL-3 MISSION

S3-A OLCI Cyclic Performance Report

Cycle No. 021

Start date: 07/08/2017

End date: 03/09/2017



*Mission
Performance
Centre*



Ref.: S3MPC.ACR.PR.01-021

Issue: 1.0

Date: 08/09/2017

Contract: 400011836/14/I-LG

Customer: ESA	Document Ref.: S3MPC.ACR.PR.01-021
Contract No.: 4000111836/14/I-LG	Date: 08/09/2017
	Issue: 1.0

Project:	PREPARATION AND OPERATIONS OF THE MISSION PERFORMANCE CENTRE (MPC) FOR THE COPERNICUS SENTINEL-3 MISSION		
Title:	S3-A OLCI Cyclic Performance Report		
Author(s):	OLCI ESLs		
Approved by:	L. Bourg, OLCI ESL Coordinator	Authorized by	Frédéric Rouffi, OPT Technical Performance Manager
Distribution:	ESA, EUMETSAT, S3MPC consortium		
Accepted by ESA	S. Dransfeld, MPC Deputy TO for OPT P. Féménias, MPC TO		
Filename	S3MPC.ACR.PR.01-021 - i1r0 - OLCI Cyclic Report 021.docx		

Disclaimer

The work performed in the frame of this contract is carried out with funding by the European Union. The views expressed herein can in no way be taken to reflect the official opinion of either the European Union or the European Space Agency.





Table of content

TABLE OF CONTENT IV

LIST OF FIGURES V

1 INSTRUMENT MONITORING 1

1.1 CCD TEMPERATURES..... 1

1.2 RADIOMETRIC CALIBRATION 2

 1.2.1 *Dark Offsets [OLCI-L1B-CV-230]* 4

 1.2.2 *Instrument response and degradation modelling [OLCI-L1B-CV-250]*..... 8

 1.2.3 *Ageing of nominal diffuser [OLCI-L1B-CV-240]*..... 15

 1.2.4 *Updating of calibration ADF [OLCI-L1B-CV-260]* 16

 1.2.5 *Radiometric Calibrations for sun azimuth angle dependency and Yaw Manoeuvres for Solar Diffuser on-orbit re-characterization [OLCI-L1B-CV-270 and OLCI-L1B-CV-280]*..... 16

1.3 SPECTRAL CALIBRATION [OLCI-L1B-CV-400]..... 16

1.4 SIGNAL TO NOISE ASSESSMENT [OLCI-L1B-CV-620] 16

 1.4.1 *SNR from Radiometric calibration data*..... 16

 1.4.2 *SNR from EO data*..... 19

1.5 GEOMETRIC CALIBRATION/VALIDATION 19

2 OLCI LEVEL 1 PRODUCT VALIDATION22

2.1 [OLCI-L1B-CV-300], [OLCI-L1B-CV-310] – RADIOMETRIC VALIDATION 22

 2.1.1 *S3ETRAC Service* 22

 2.1.2 *Radiometric validation with DIMITRI* 23

 2.1.3 *Radiometric validation with OSCAR* 28

2.2 [OLCI-L1B-CV-320] – RADIOMETRIC VALIDATION WITH LEVEL 3 PRODUCTS..... 29

3 LEVEL 2 LAND PRODUCTS VALIDATION30

3.1 [OLCI-L2LRF-CV-300]..... 30

3.2 [OLCI-L2LRF-CV-410 & OLCI-L2LRF-CV-420] – CLOUD MASKING & SURFACE CLASSIFICATION FOR LAND PRODUCTS 38

3.3 VALIDATION OF INTEGRATED WATER VAPOUR OVER LAND 38

4 LEVEL 2 WATER PRODUCTS VALIDATION39

4.1 [OLCI-L2-CV-210, OLCI-L2-CV-220] – VICARIOUS CALIBRATION OF THE NIR AND VIS BANDS..... 39

4.2 [OLCI-L2WLR-CV-300, OLCI-L2WLR-CV-310, OLCI-L2WLR-CV-32, OLCI-L2WLR-CV-330, OLCI-L2WLR-CV-340, OLCI-L2WLR-CV-350, OLCI-L2WLR-CV-360 AND OLCI-L2WLR-CV-370] – LEVEL 2 WATER-LEAVING REFLECTANCE PRODUCT VALIDATION..... 39

4.3 [OLCI-L2WLR-CV530] VALIDATION OF AEROSOL PRODUCT..... 45

5 LEVEL 2 SYN PRODUCTS VALIDATION.....46

5.1 [SYN-L2-CV-100] 46

6 EVENTS54

7 APPENDIX A55

	<p>Sentinel-3 MPC</p> <p>S3-A OLCI Cyclic Performance Report</p> <p>Cycle No. 021</p>	<p>Ref.: S3MPC.ACR.PR.01-021</p> <p>Issue: 1.0</p> <p>Date: 08/09/2017</p> <p>Page: v</p>
--	--	---

List of Figures

Figure 1: long term monitoring of CCD temperatures using minimum value (top), time averaged values (middle), and maximum value (bottom) provided in the annotations of the Radiometric Calibration Level 1 products, for the Shutter frames, all radiometric calibrations so far. ----- 1

Figure 2: Same as Figure 1 for diffuser frames. ----- 2

Figure 3: Sun azimuth angles during acquired Radiometric Calibrations (diffuser frame) on top of nominal yearly cycle (black curve). Diffuser 1 with diamonds, diffuser 2 with crosses, 2016 acquisitions in blue, 2017 in red. ----- 3

Figure 4: Sun geometry during radiometric Calibrations on top of characterization ones (diffuser frame) 3

Figure 5: Dark Offset table for band Oa06 with (red) and without (black) HEP filtering (Radiometric Calibration of 22 July 2017). The strong HEP event near pixel 400 has been detected and removed by the HEP filtering. ----- 4

Figure 6: Dark Offset for band Oa1 (top) and Oa21 (bottom), all radiometric calibrations so far except the first one (orbit 183) for which the instrument was not thermally stable yet. ----- 5

Figure 7: map of periodic noise for the 5 cameras, for band Oa21. X-axis is detector number (East part, from 540 to 740, where the periodic noise occurs), Y-axis is the orbit number. The counts have been corrected from the west detectors mean value (not affected by periodic noise) in order to remove mean level gaps and consequently to have a better visualisation of the long term evolution of the periodic noise structure. Periodic noise amplitude is high in camera 2, 3 and 4. It is lower in camera 4 and small in camera 1. ----- 6

Figure 8: Dark Current for band Oa1 (top) and Oa21 (bottom), all radiometric calibrations so far except the first one (orbit 183) for which the instrument was not thermally stable yet. ----- 7

Figure 9: left column: ACT mean on 400 first detectors of Dark Current coefficients for spectral band Oa01 (top) and Oa21 (bottom). Right column: same as left column but for Standard deviation instead of mean. We see an increase of the DC level as a function of time especially for band Oa21. A possible explanation could be the increase of the number of hot pixels which is more important in Oa21 because this band is made of more CCD lines than band Oa01 and thus receives more cosmic rays impacts. It is known that cosmic rays degrade the structure of the CCD, generating more and more hot pixels at long term scales. ----- 7

Figure 10: Gain Coefficients for band Oa1 (top) and Oa21 (bottom), all diffuser 1 radiometric calibrations so far except the first one (orbit 183) for which the instrument was not thermally stable yet. ----- 8

Figure 11: camera averaged gain relative evolution with respect to “best geometry” calibration (22/11), as a function of elapsed time since launch; one curve for each band (see colour code on plots), one plot for each module. The star tracker anomaly fix (6/04/16) is represented by a vertical red dashed line. ---- 9

Figure 12: Camera-averaged instrument evolution since channel programming change (25/04/2016) and up to most recent calibration (27/08/2017) versus wavelength. -----10

	Sentinel-3 MPC S3-A OLCI Cyclic Performance Report Cycle No. 021	Ref.: S3MPC.ACR.PR.01-021 Issue: 1.0 Date: 08/09/2017 Page: vi
--	---	---

Figure 13: For the 5 cameras: Evolution model performance, as camera-average and standard deviation of ratio of Model over Data vs. wavelength, for each orbit of the test dataset, including 14 calibration in extrapolation, with a colour code for each calibration from blue (oldest) to red (most recent).-----11

Figure 14: model performance: ratio of model over data for all pixels (x axis) of all orbits (y axis), for channel Oa4. The outlying orbit #40 is that of 31/03/2017. -----12

Figure 15: Evolution model performance, as ratio of Model over Data vs. pixels, all cameras side by side, over the whole current calibration dataset (since instrument programming update), including 8 calibration in extrapolation, channels Oa1 to Oa6. -----13

Figure 16: same as Figure 14 for channels Oa7 to Oa14. -----14

Figure 17: same as Figure 15 for channels Oa15 to Oa21.-----15

Figure 18: Signal to Noise ratio as a function of the spectral band for the 5 cameras. These results have been computed from radiometric calibration data. All calibrations except first one (orbit 183) are presents with the colours corresponding to the orbit number (see legend). The SNR is very stable with time: the curves for all orbits are almost superimposed. The dashed curve is the ESA requirement. ----17

Figure 19: long-term stability of the SNR estimates from Calibration data, example of channel Oa1. ----18

Figure 20: histograms of geolocation errors for the along-track (left) and across-track (right) directions, example 20/08/2017.-----20

Figure 21: georeferencing error in along-track (left) and across-track (right) directions for all the GCPs, example of 20/08/2017. -----20

Figure 22: time series of geolocation errors for the along-track (blue) and across-track (red) directions over 15.6 months. -----21

Figure 23: summary of S3ETRAC products generation for OLCI (number of OLCI L1 products Ingested, yellow – number of S3ETRAC extracted products generated, blue – number of S3ETRAC runs without generation of output product (data not meeting selection requirements), green – number of runs ending in error, red, one plot per site type). -----23

Figure 24: Time-series of the elementary ratios (observed/simulated) signal from S3A/OLCI for (top to bottom) bands Oa03, Oa8 and Oa17 respectively over Six PICS Cal/Val sites. Dashed-green and orange lines indicate the 2% and 5% respectively. Error bars indicate the desert methodology uncertainty. ----24

Figure 25: The estimated gain values for S3A/OLCI over the 6 PICS sites identified by CEOS over the period April 2016 – July 2017 as a function of wavelength. Dashed-green and orange lines indicate the 2% and 5% respectively. Error bars indicate the desert methodology uncertainty. -----25

Figure 26: Time-series of the elementary ratios (observed/simulated) signal from (black) S2A/MSI, (blue) S3A/OLCI and (Cyan) Aqua/MODIS for (band Oa17: 865nm and Oa08: 665 nm over ALGERIA5 and LIBYA1 sites. Dashed-green and orange lines indicate the 2% and 5% respectively. Error bars indicate the desert methodology uncertainty. -----26

Figure 27: The estimated gain values (observed-signal /simulated-signal) averaged over different period from different sensors over PICS as function of wavelength.-----27

	Sentinel-3 MPC S3-A OLCI Cyclic Performance Report Cycle No. 021	Ref.: S3MPC.ACR.PR.01-021 Issue: 1.0 Date: 08/09/2017 Page: vii
--	---	--

Figure 28: The estimated gain values for S3A/OLCI over the 6 Ocean CalVal sites (Atl-NW_Optimum, Atl-SW_Optimum, Pac-NE_Optimum, Pac-NW_Optimum, SPG_Optimum and SIO_Optimum) over the period December 2016 – September 2017 as a function of wavelength. Dashed-green, and orange lines indicate the 2%, 5% respectively. Error bars indicate the methodology uncertainty. -----27

Figure-29 : The estimated gain values for S3A/OLCI from Glint, Rayleigh, and PICS over the period March 2016 – August 2017 for PICS and December 2016-September 2017 for Rayleigh and December 2016-July 2017 Glint methods as a function of wavelength. We use the gain value of Oa8 from PICS method as reference gain for Glint. Dashed-green and orange lines indicate the 2% and 5% respectively. Error bars indicate the methods uncertainties. -----28

Figure 30: OSCAR Rayleigh results for May and June 2017. -----29

Figure 31 Sampling strategy -----31

Figure 32 False Colour Composition (Band combination: 8,4,3) of the study region, Utiel can be seen in the bottom right corner of the image. -----31

Figure 33: DEGeb time series -----32

Figure 34: ITCat time series -----33

Figure 35: ITIsp time series -----33

Figure 36: ITSro time series -----34

Figure 37: ITTra time series -----34

Figure 38: ITTra, OGVI on 20170702 (left) and 20170703 (right) -----35

Figure 39: ITTra, OGVI on 20170706 (left) and 20170707 (right) -----35

Figure 40: SPAlI time series -----35

Figure 41: SPVal time series -----36

Figure 42: UKNfo time series -----36

Figure 43: USNe1 time series -----37

Figure 44: USNe2 time series -----37

Figure 45: USNe3 time series -----38

Figure 46: Scatter plots of OLCI versus in situ radiometry (FR data) -----40

Figure 47: OLCI and AERONET-OC radiometric time series at 490nm. -----43

Figure 48: OLCI and AERONET-OC radiometric time series at 490nm. -----44

Figure 49 : OLCI RGB image from S3A_OL_1_EFR___20170619T101637_20170619T101937_20170619T122047_0179_019_065_2160_SV L_O_NR_002.SEN3 -----46

Figure 50: Maps and histogram of AOT@550 nm from associated SYN product; S3A_SY_2_SYN___20170619T101637_20170619T101937_20170621T033649_0179_019_065_2160_LN 2_O_NT_002.SEN3 -----47

	<p>Sentinel-3 MPC</p> <p>S3-A OLCI Cyclic Performance Report</p> <p>Cycle No. 021</p>	<p>Ref.: S3MPC.ACR.PR.01-021</p> <p>Issue: 1.0</p> <p>Date: 08/09/2017</p> <p>Page: viii</p>
--	--	--

Figure 51 : Surface directional Reflectance associated with different OLCI and SLSTR channels from S3A_SY_2_SYN___20170619T101637_20170619T101937_20170621T033649_0179_019_065_2160_LN 2_O_NT_002.SEN3. The unfilled land pixels are the one associated with a negative surface directional reflectance -----47

Figure 52 : (a) RGB image of the SLSTR Nadir view and (b) SYN L2 Aerosol Optical Thickness obtained with current SYN L2 IPF from S3A_SL_1_RBT___20170227T003224_20170227T003524_20170329T135202_0180_015_002____LR 1_D_NT_001.SEN3 -----48

Figure 53 : TOA radiances associated with SLSTR S4 channel and used in the SYN L2 Aerosol retrieval---48

Figure 54 : Maps and histogram of AOT@550 nm from SYN product; S3A_SY_2_SYN___20170619T101637_20170619T101937_REPROCESSED without SLSTR S4 taken into account in the aerosol retrieval -----49

Figure 55 : Surface directional Reflectance associated with different OLCI and SLSTR channels from S3A_SY_2_SYN___20170619T101637_20170619T101937_REPROCESSED without SLSTR S4 channel taken into account in the aerosol retrieval section -----50

Figure 56 : Analysis of the Aerosol retrieval outputs from S3A_SY_2_SYN___20170227T003224_20170227T003524_REPROCESSED -----51

Figure 57 : Resulting Aerosol Optical Thickness @550 nm from S3A_SY_2_SYN___20170227T003224_20170227T003524_REPROCESSED using different configurations -----52

Figure 58 : Observation angles associated with each contribution of SYN L2 aerosol retrieval section ---53



1 Instrument monitoring

1.1 CCD temperatures

The monitoring of the CCD temperatures is based on MPMF data extractions not yet operational. In the meantime, we monitor the CCD temperatures on the long-term using Radiometric Calibration Annotations (see Figure 1). Variations are very small (0.09 C peak-to-peak) and no trend can be identified. Data from current cycle (rightmost data points) do not show any specificity.

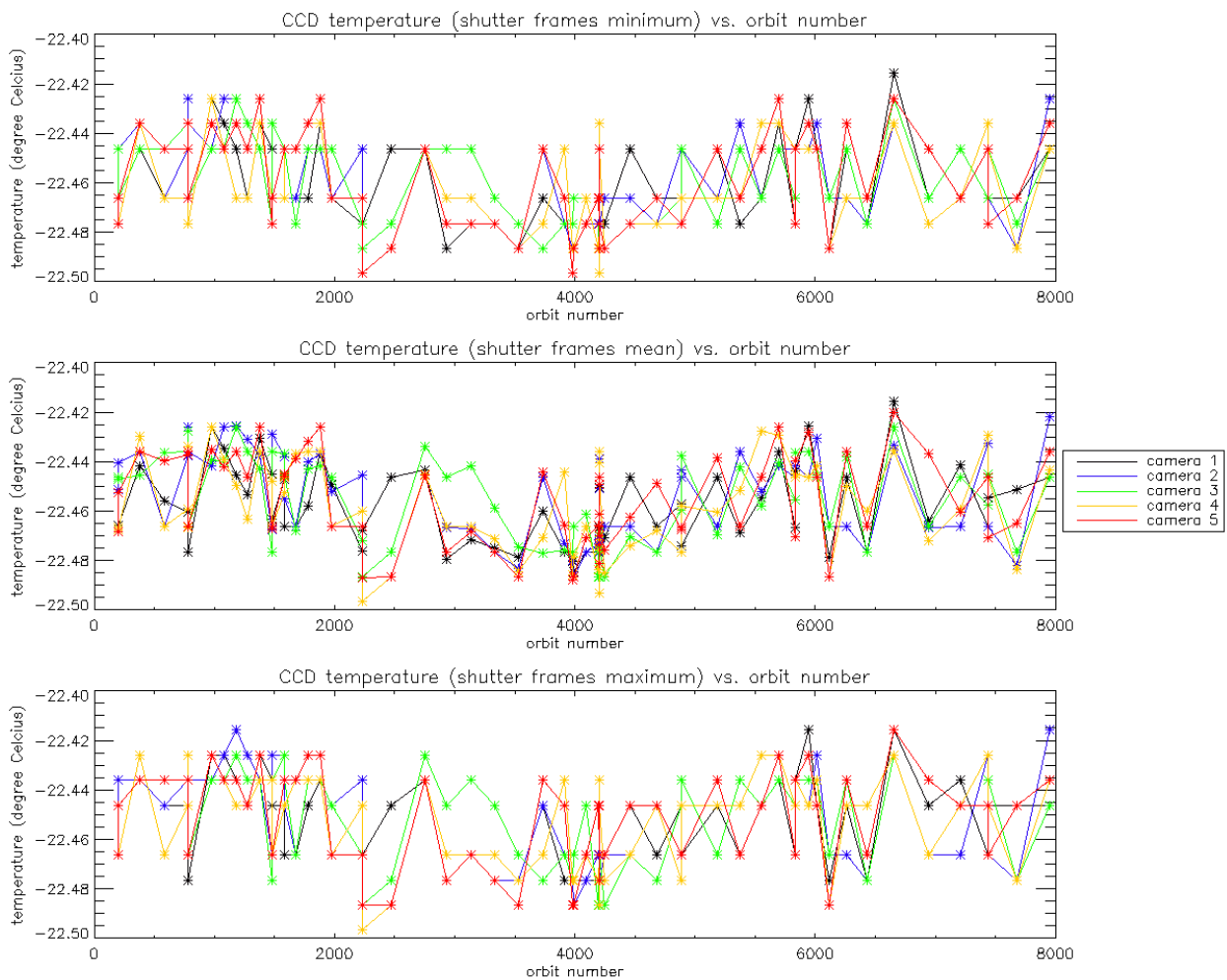


Figure 1: long term monitoring of CCD temperatures using minimum value (top), time averaged values (middle), and maximum value (bottom) provided in the annotations of the Radiometric Calibration Level 1 products, for the Shutter frames, all radiometric calibrations so far.

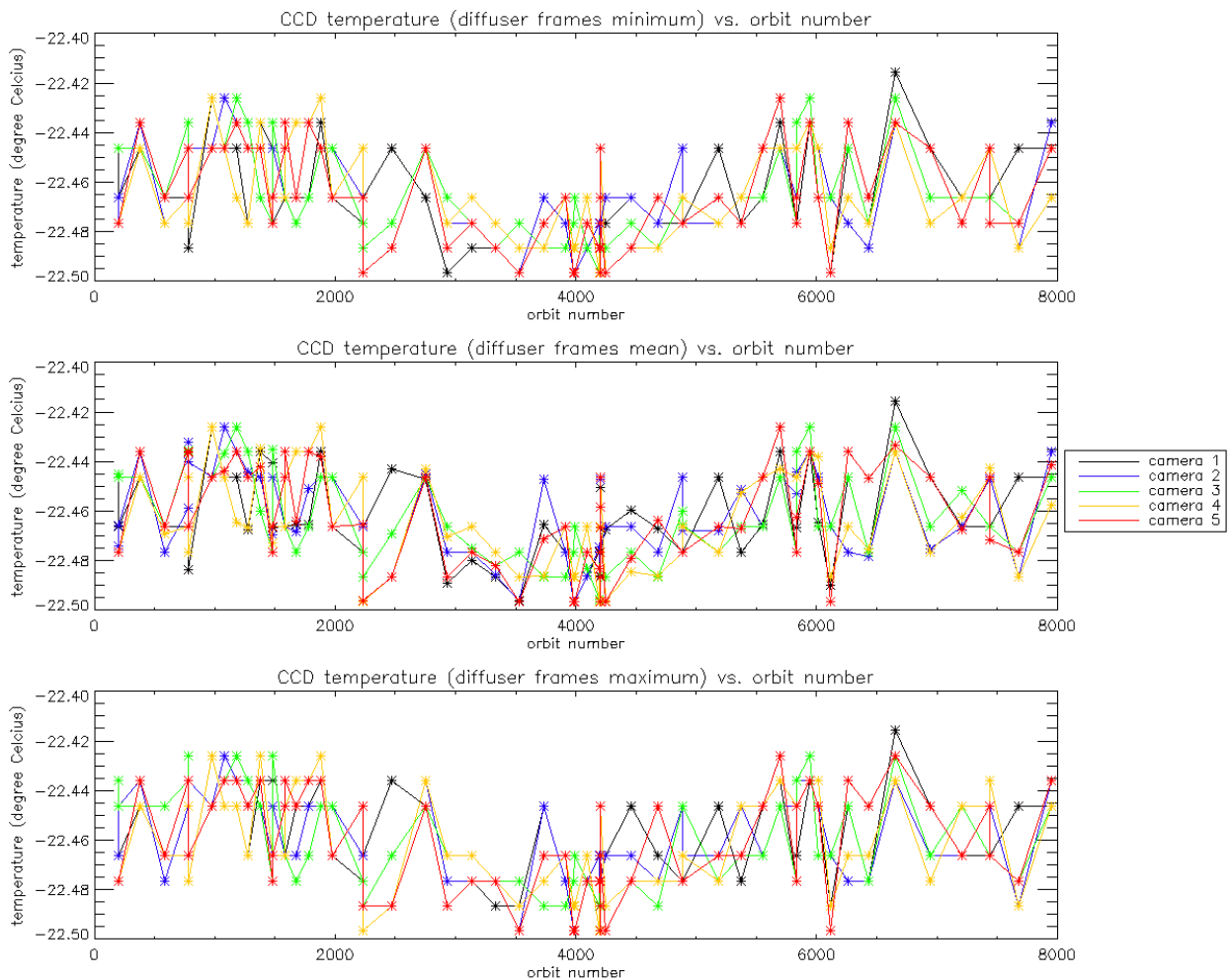


Figure 2: Same as Figure 1 for diffuser frames.

1.2 Radiometric Calibration

Two OLCI Radiometric Calibration Sequences have been acquired during Cycle 021:

- ❖ S01 sequence (diffuser 1) on 08/08/2017 07:29 to 07:31 (absolute orbit 7679)
- ❖ S01 sequence (diffuser 1) on 27/08/2017 14:22 to 14:24 (absolute orbit 7954)

The acquired Sun azimuth angles are presented on below, on top of the nominal values without Yaw Manoeuvre (i.e. with nominal Yaw Steering control of the satellite).



Sentinel-3 MPC
S3-A OLCI Cyclic Performance Report
Cycle No. 021

Ref.: S3MPC.ACR.PR.01-021
 Issue: 1.0
 Date: 08/09/2017
 Page: 3

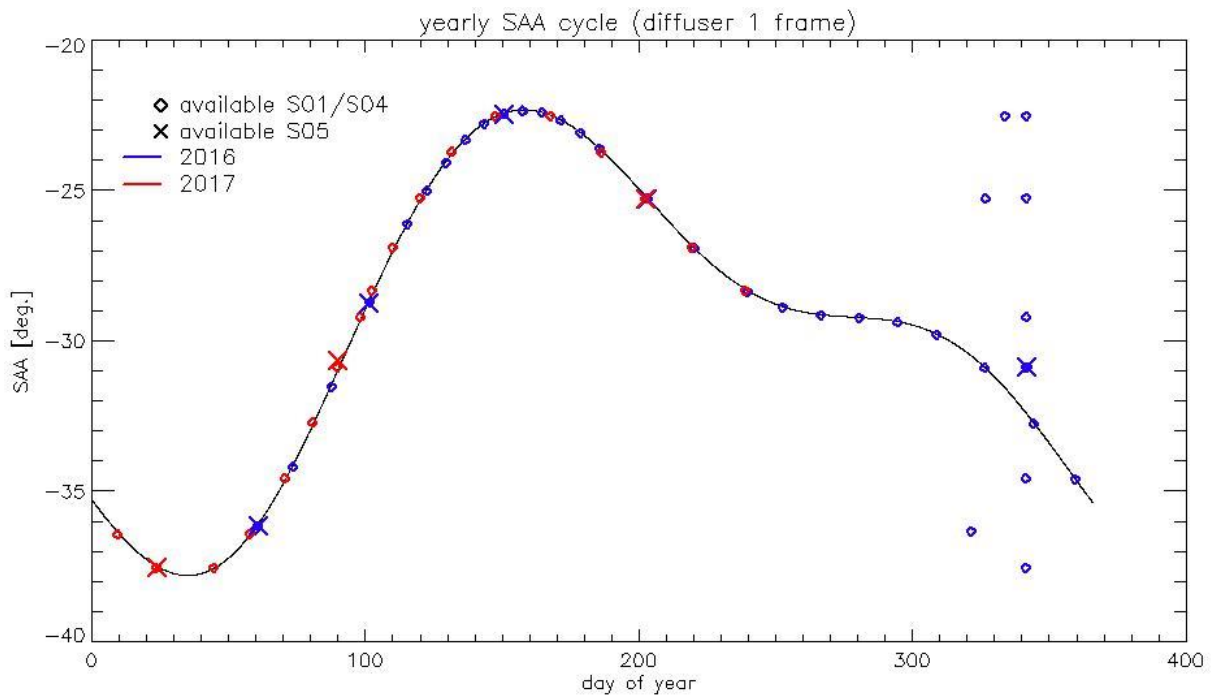


Figure 3: Sun azimuth angles during acquired Radiometric Calibrations (diffuser frame) on top of nominal yearly cycle (black curve). Diffuser 1 with diamonds, diffuser 2 with crosses, 2016 acquisitions in blue, 2017 in red.

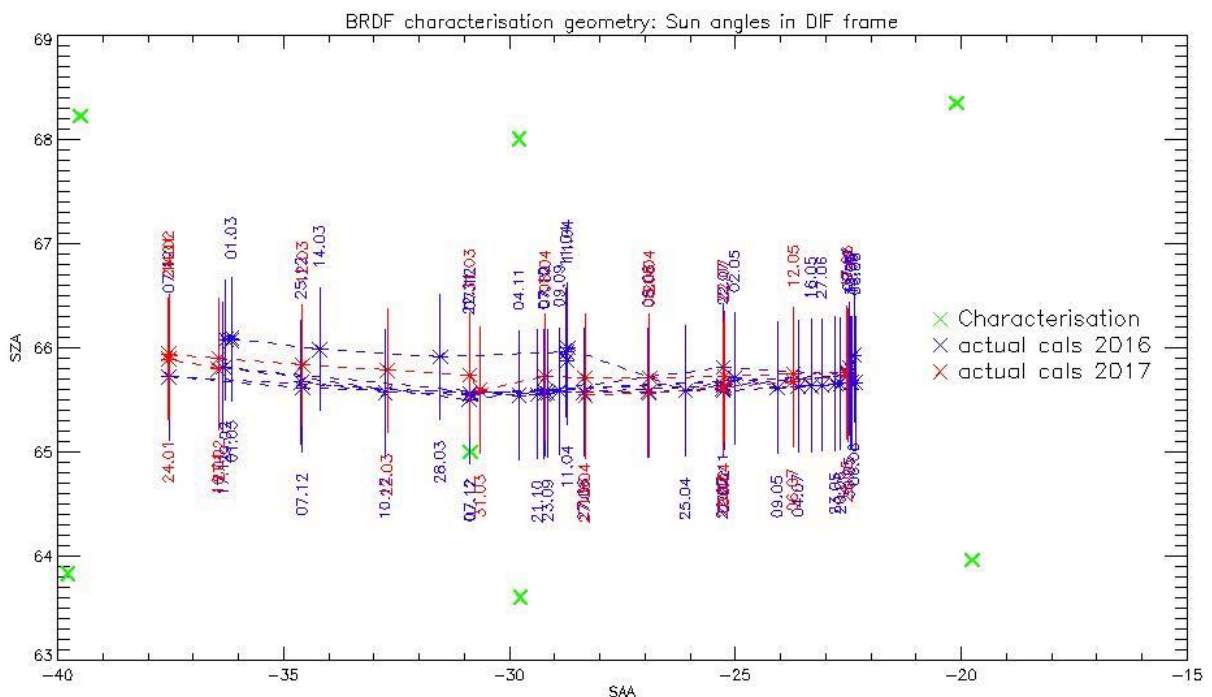


Figure 4: Sun geometry during radiometric Calibrations on top of characterization ones (diffuser frame)

This section presents the overall monitoring of the parameters derived from radiometric calibration data and highlights, if present, specificity of current cycle data.

1.2.1 Dark Offsets [OLCI-L1B-CV-230]

Note about the High Energy Particles:

The filtering of High Energy Particle (HEP) events from radiometric calibration data has been implemented (for shutter frames only) in a post processor, allowing generating Dark Offset and Dark Current tables computed on filtered data. The post-processor starts from IPF intermediate data (corrected counts), applies the HEP detection and filtering and finally computes the Dark Offset and Dark Current tables the same way as IPF. An example of the impact of HEP filtering is given in Figure 5.

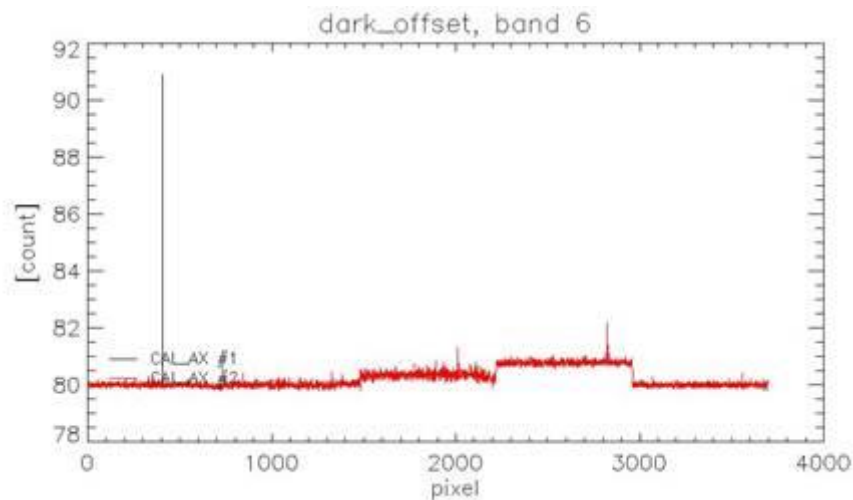


Figure 5: Dark Offset table for band Oa06 with (red) and without (black) HEP filtering (Radiometric Calibration of 22 July 2017). The strong HEP event near pixel 400 has been detected and removed by the HEP filtering.

All results presented below in this section have been obtained using the HEP filtered Dark Offset and Dark Current tables.

Dark offsets

Dark offsets are continuously affected by the global offset induced by the Periodic Noise on the OCL convergence. Current Cycle calibrations are affected the same way as others. The amplitude of the shift varies with band and camera from virtually nothing (e.g. camera 2, band Oa1) to up to 5 counts (Oa21, camera 3). The Periodic Noise itself comes on top of the global shift with its known signature: high frequency oscillations with a rapid damp. This effect remains more or less stable with time in terms of amplitude, frequency and decay length, but its phase varies with time, introducing the global offset mentioned above.



Sentinel-3 MPC
S3-A OLCI Cyclic Performance Report
Cycle No. 021

Ref.: S3MPC.ACR.PR.01-021
Issue: 1.0
Date: 08/09/2017
Page: 5

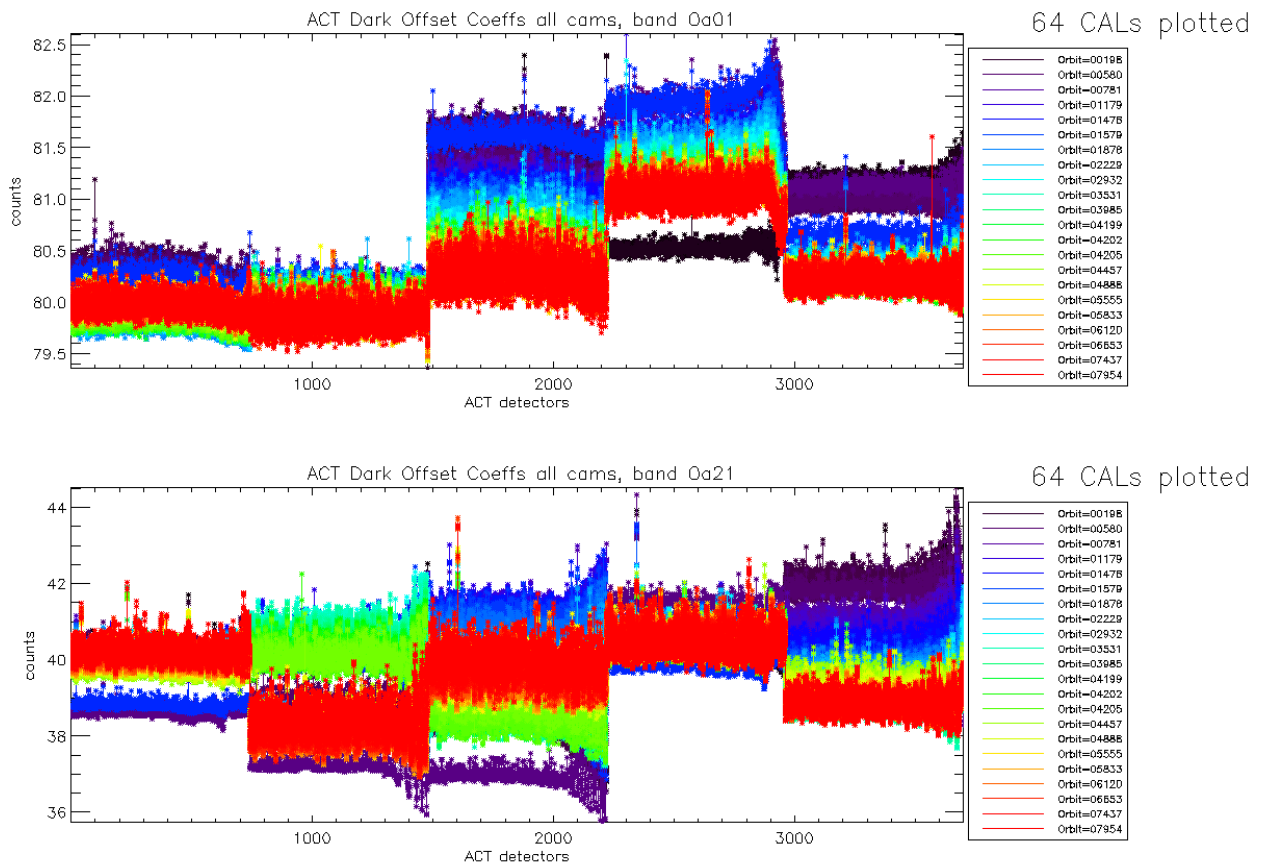


Figure 6: Dark Offset for band Oa1 (top) and Oa21 (bottom), all radiometric calibrations so far except the first one (orbit 183) for which the instrument was not thermally stable yet.

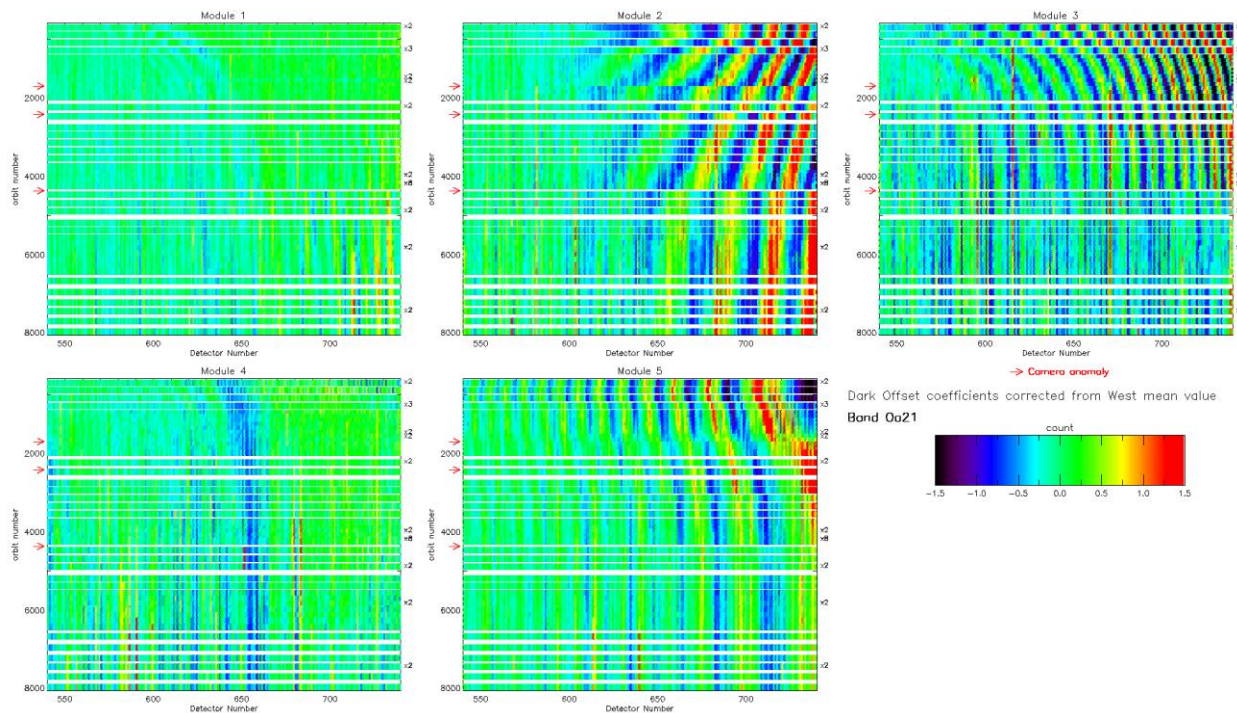


Figure 7: map of periodic noise for the 5 cameras, for band Oa21. X-axis is detector number (East part, from 540 to 740, where the periodic noise occurs), Y-axis is the orbit number. The counts have been corrected from the west detectors mean value (not affected by periodic noise) in order to remove mean level gaps and consequently to have a better visualisation of the long term evolution of the periodic noise structure. Periodic noise amplitude is high in camera 2, 3 and 4. It is lower in camera 4 and small in camera 1.

Looking at Figure 6 shows no significant evolution of this parameter during the current cycle. Figure 7 shows that since the last sudden PN change (phase and amplitude) caused by the camera-2 anomaly at orbit 4364 (18 December 2016), PN is nearly stabilized again. (See in particular cameras 2, 3 & 5).

Dark Currents

Dark Currents are not affected by the global offset of the Dark Offsets, thanks to the clamping to the average blind pixels value. However, the oscillations of Periodic Noise remain visible. There is no significant evolution of this parameter during the current cycle.

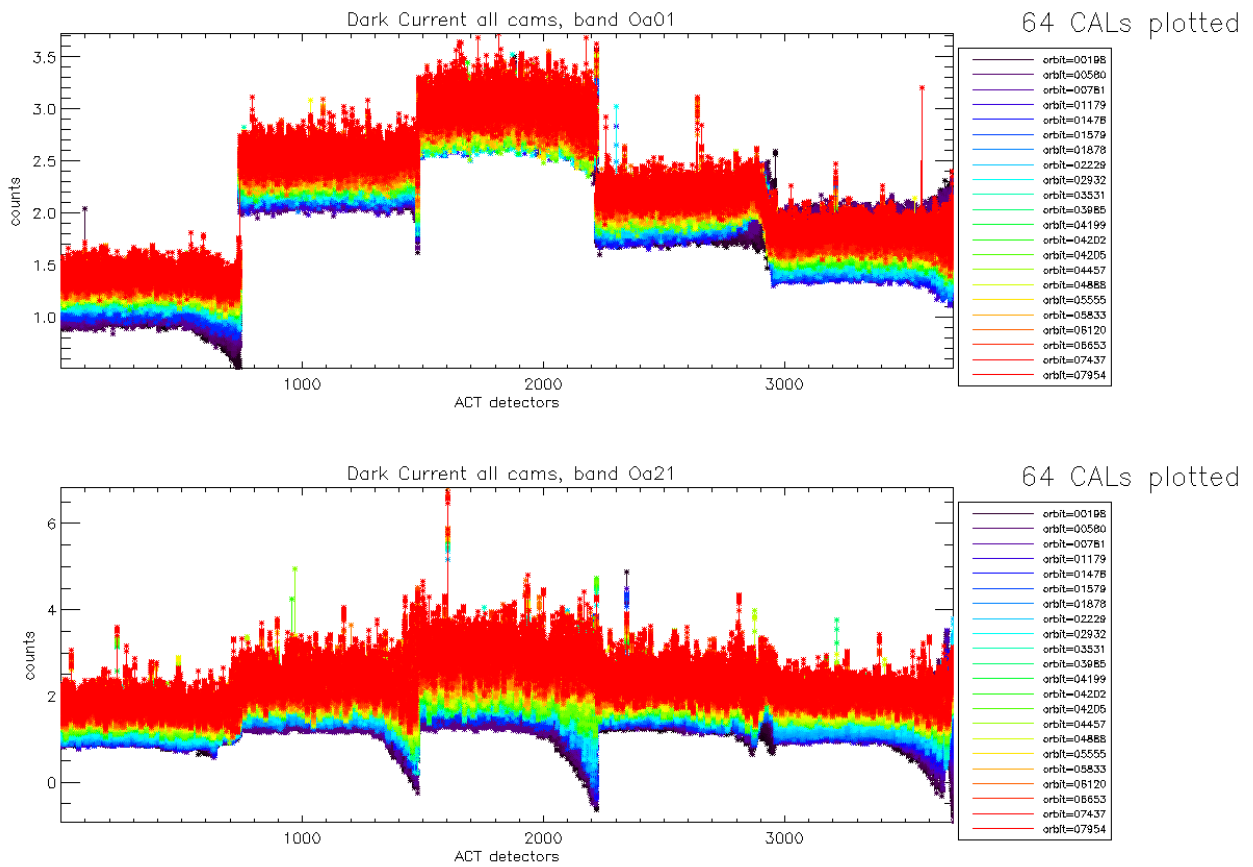


Figure 8: Dark Current for band Oa1 (top) and Oa21 (bottom), all radiometric calibrations so far except the first one (orbit 183) for which the instrument was not thermally stable yet.

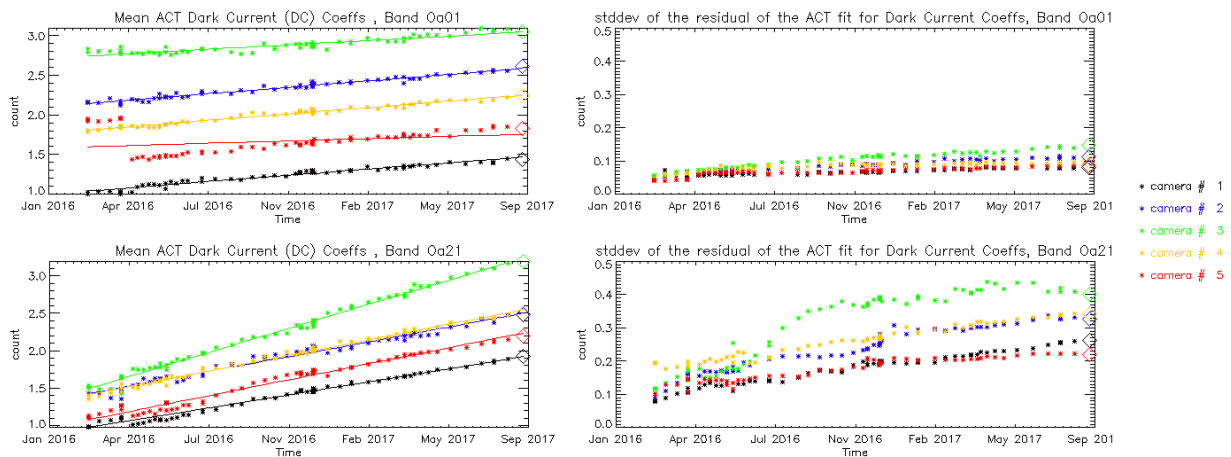


Figure 9: left column: ACT mean on 400 first detectors of Dark Current coefficients for spectral band Oa01 (top) and Oa21 (bottom). Right column: same as left column but for Standard deviation instead of mean. We see an increase of the DC level as a function of time especially for band Oa21. A possible explanation could be the increase of the number of hot pixels which is more important in Oa21 because this band is made of more CCD lines than band Oa01 and thus receives more cosmic rays impacts. It is known that cosmic rays degrade the structure of the CCD, generating more and more hot pixels at long term scales.



1.2.2 Instrument response and degradation modelling [OLCI-L1B-CV-250]

1.2.2.1 Instrument response monitoring

Figure 10 below shows the gain coefficients of every pixel for two OLCI channels, Oa1 (400 nm) and Oa21 (1020 nm), highlighting the significant evolution of the instrument response since early mission.

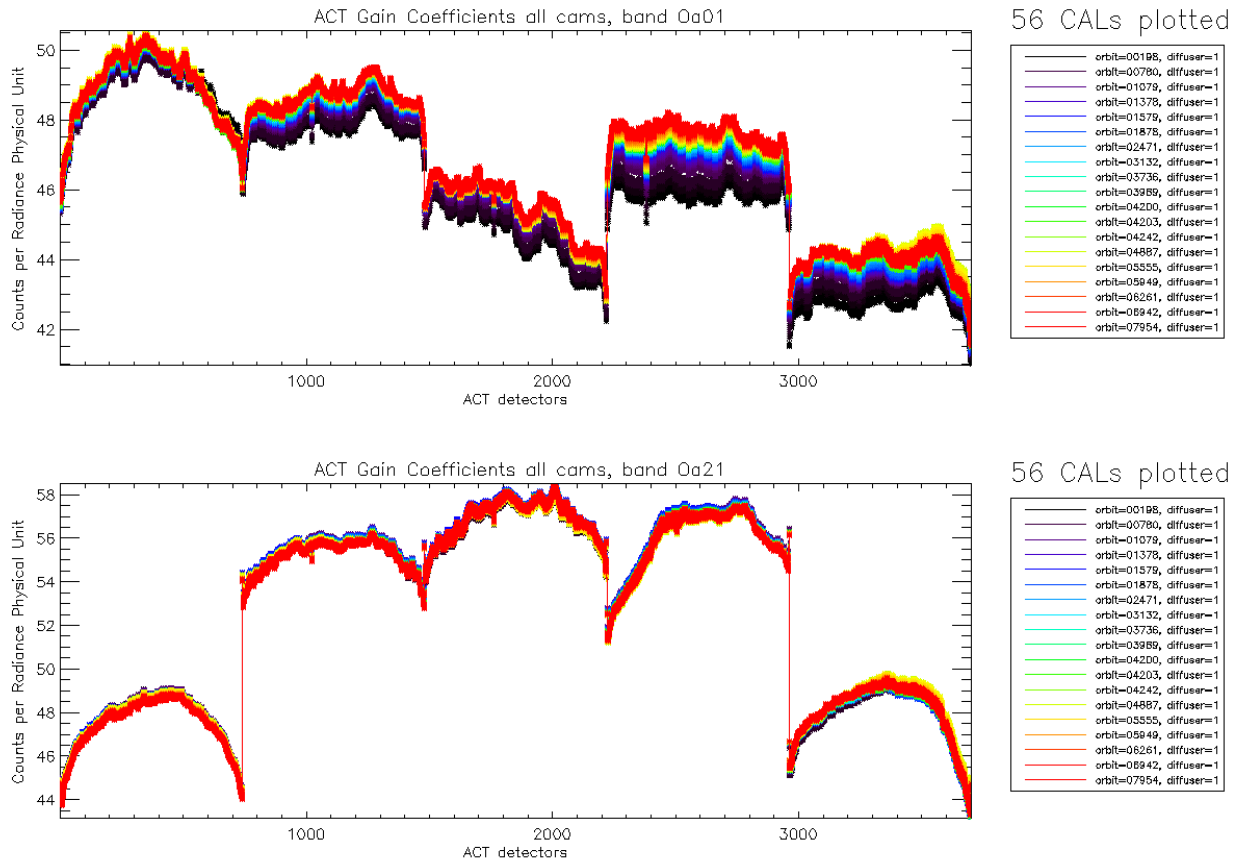


Figure 10: Gain Coefficients for band Oa1 (top) and Oa21 (bottom), all diffuser 1 radiometric calibrations so far except the first one (orbit 183) for which the instrument was not thermally stable yet.

The gains plotted in Figure 10, however are derived using the ground BRDF model – as the only one available in the operational processing software so far – which is known to suffer from illumination geometry dependent residual errors (see previous Cyclic Reports for more details). Consequently they are post-processed to replace the ground BRDF model by the in-flight version, based on Yaw Manoeuvres data, prior to determine the radiometric evolution.

Figure 11 displays a summary of the time evolution derived from post-processed gains: the cross-track average of the BRDF corrected gains is plotted as a function of time, for each module, relative to a given reference calibration (the 12/12/2016). It shows that, if a significant evolution occurred during the early mission, the trends tend to stabilize, with the exception of band 1 of camera 4.

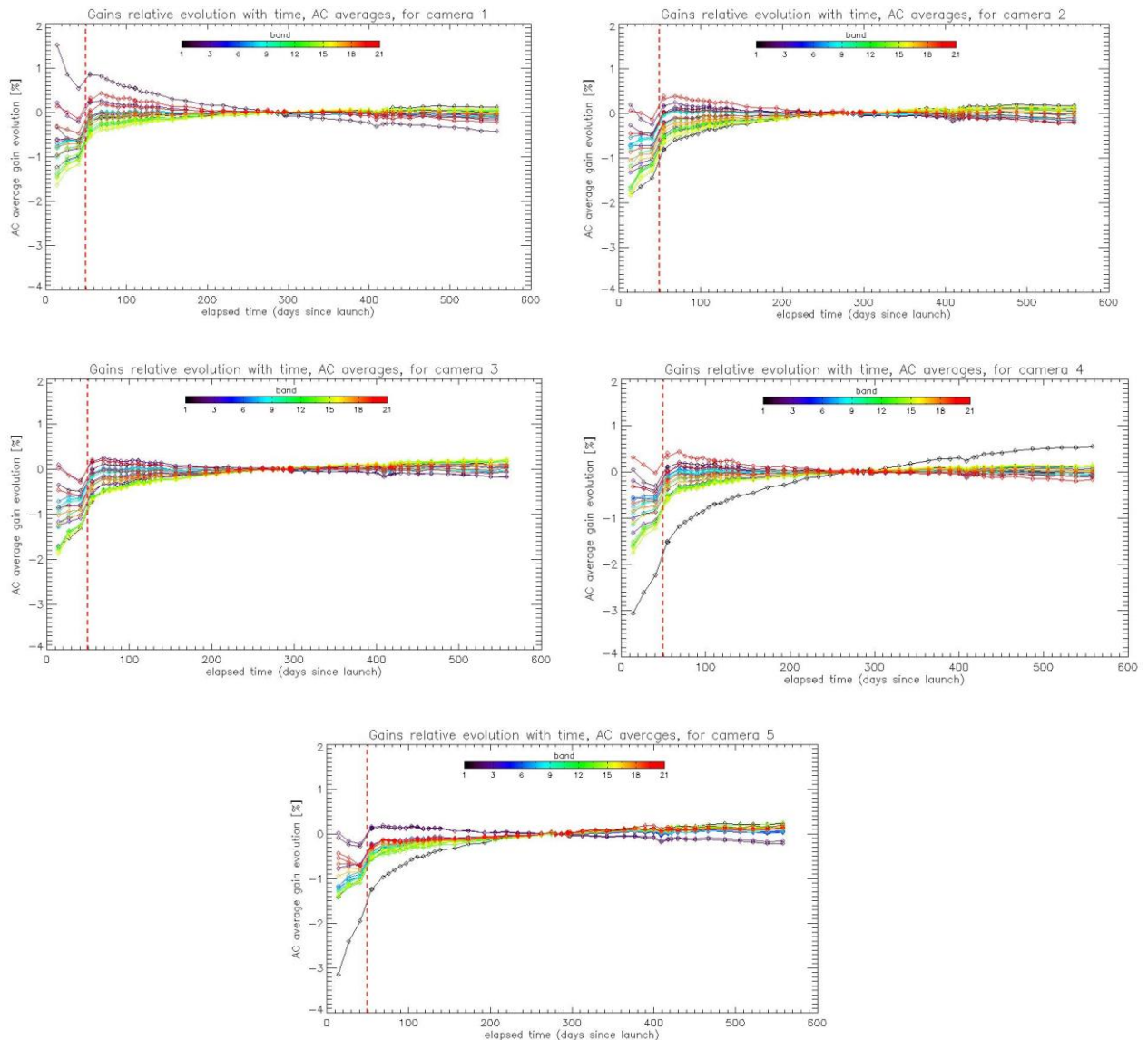


Figure 11: camera averaged gain relative evolution with respect to “best geometry” calibration (22/11), as a function of elapsed time since launch; one curve for each band (see colour code on plots), one plot for each module. The star tracker anomaly fix (6/04/16) is represented by a vertical red dashed line.

The behaviour over the first two months of mission, really different and highlighted by Figure 11, is explained by the Star Tracker software anomaly during which the attitude information provided by the platform was corrupted, preventing to compute a correct illumination geometry, with a significant impact on the gain computation.

1.2.2.2 Instrument evolution modelling

Thanks to the work done on the Yaw Manoeuvres Calibration acquisitions (see section 1.2.5) an upgraded diffuser BRDF model has been derived, allowing to get rid of the operational model dependency with Sun azimuth discussed above. This in turn allowed building a global gain database

corrected for BRDF error residuals. This database was used as the basis for the derivation of a long-term radiometric drift model.

This required a number of adaptations of the dedicated software for several reasons:

- 1) The upgraded BRDF model is not implemented in the Calibration processing software (IPF OL1-RC), thus the derived gains have to be corrected for BRDF in a post-processing step, on the (justified) assumption that the BRDF changes have a second order impact on the stray-light computation.
- 2) The observed instrument evolution does not follow the expected behaviour: a slow and smooth instrument sensitivity decrease, but on the contrary can show increase as well (see Figure 12))
- 3) The time period is not long enough to correctly model the evolution for cameras/channels for which it is very small: in this case the signal to noise ratio (e. g. due to diffuser speckle) is not high enough and the fit parameters that provide the best match are not physical. As a consequence, it may happen that, despite the model matches very well to the data, its use in extrapolation generates huge drifts that are very unlikely to occur. A post-processing is thus necessary to identify and update those cases.

The model has been derived from the dataset ranging from 26/04/2016 to 12/03/2017, so that the validation dataset now includes 14 calibrations over 5.5 months for performance estimation, including the calibrations acquired during current cycle.

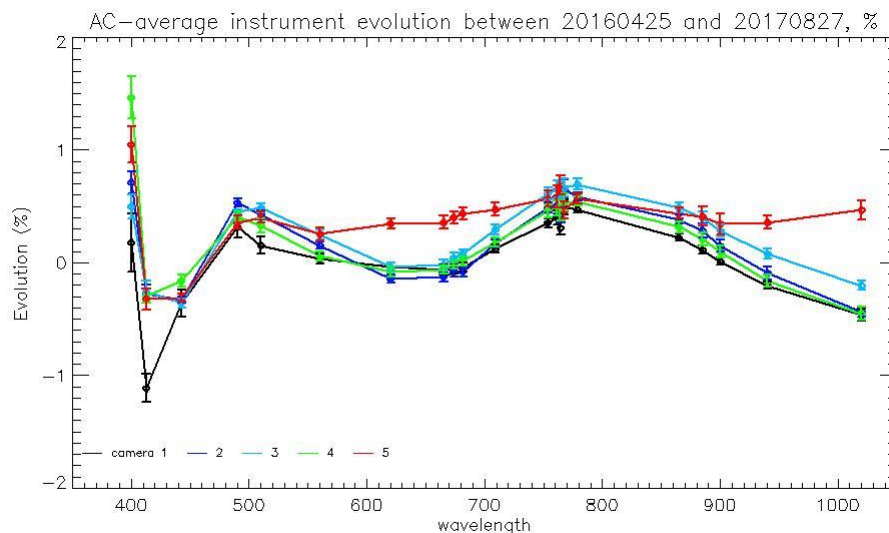


Figure 12: Camera-averaged instrument evolution since channel programming change (25/04/2016) and up to most recent calibration (27/08/2017) versus wavelength.

Once these steps are completed, the model performance over the complete dataset (including 14 calibrations in extrapolation over up to 5.5 months) is better than 0.2% except at very specific cases: few isolated pixels in about half of the bands, and two specific features in camera 5 for channels Oa8 and Oa21 that cannot be fitted with a bounded exponential model. The overall performance at each orbit is



shown on Figure 13 as the average and standard deviation of the model over data ratio as a function of wavelength, for each orbit in order to highlight a possible extrapolation issue. If the figure shows an outlying orbit, it must be stressed that it is NOT the most recent, excluding a systematic drift in extrapolation, as proved by Figure 14.

Finally, Figure 15 to Figure 17 show the detail of the model performance, with across-track plots of the model over data ratios at each orbit, one plot for each channel.

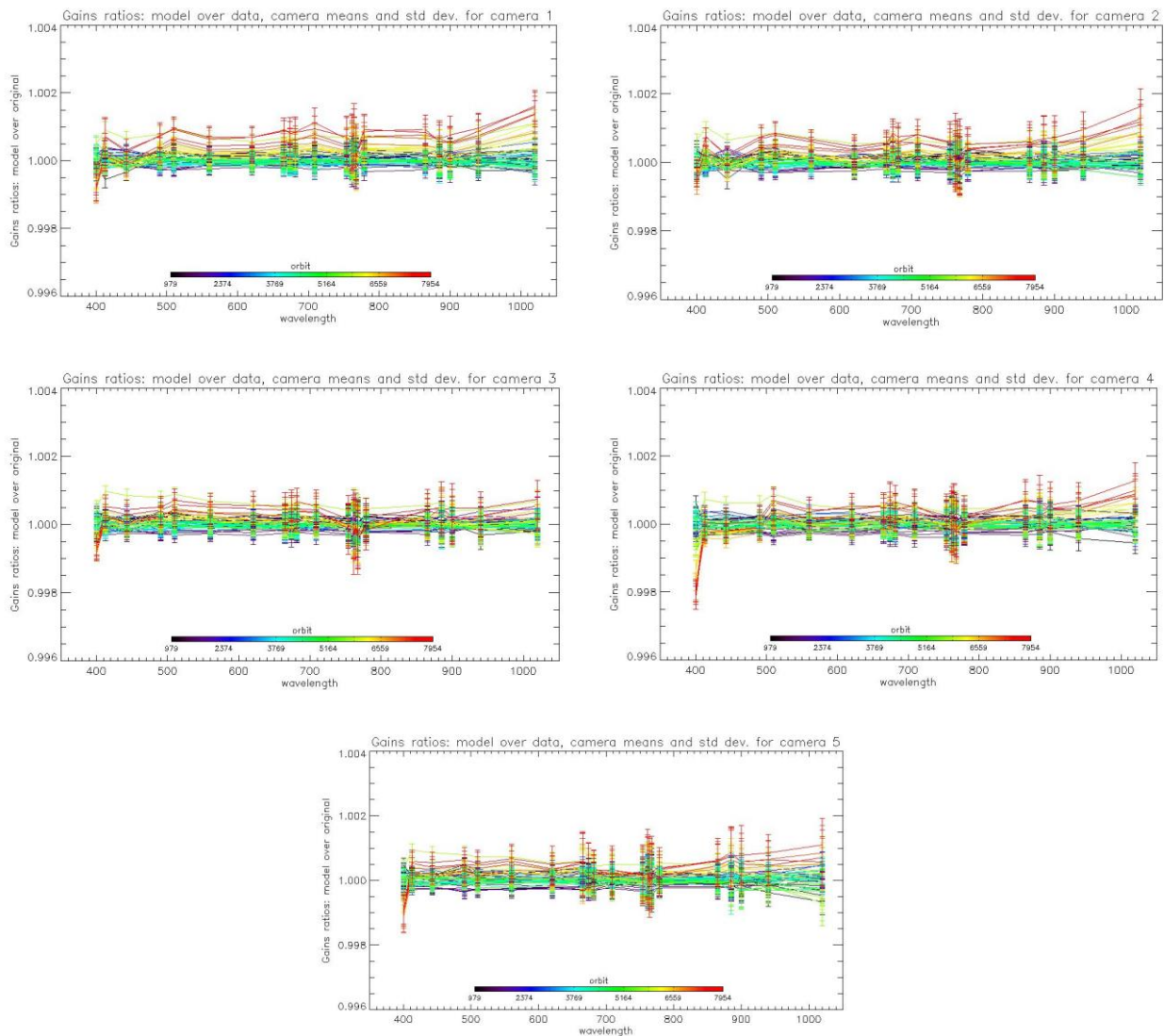


Figure 13: For the 5 cameras: Evolution model performance, as camera-average and standard deviation of ratio of Model over Data vs. wavelength, for each orbit of the test dataset, including 14 calibration in extrapolation, with a colour code for each calibration from blue (oldest) to red (most recent).

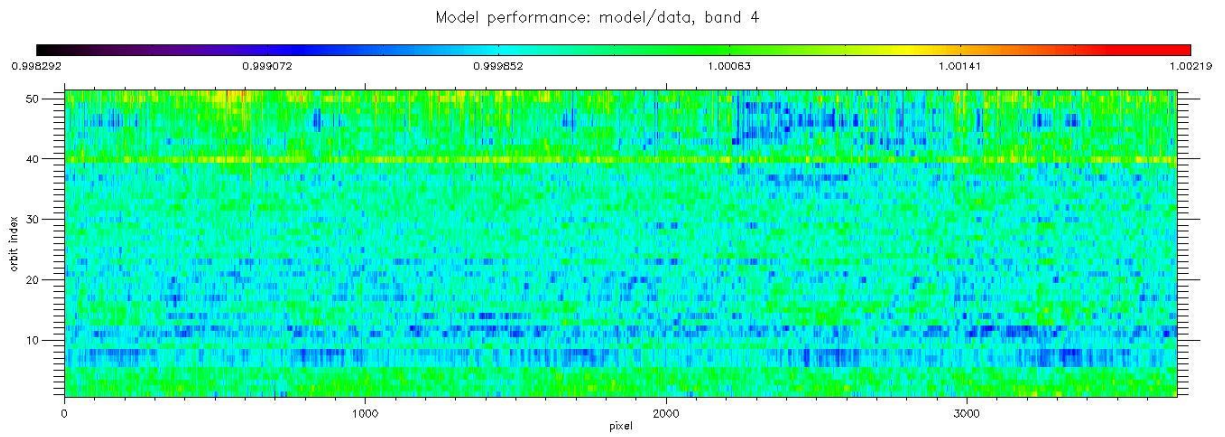


Figure 14: model performance: ratio of model over data for all pixels (x axis) of all orbits (y axis), for channel Oa4. The outlying orbit #40 is that of 31/03/2017.

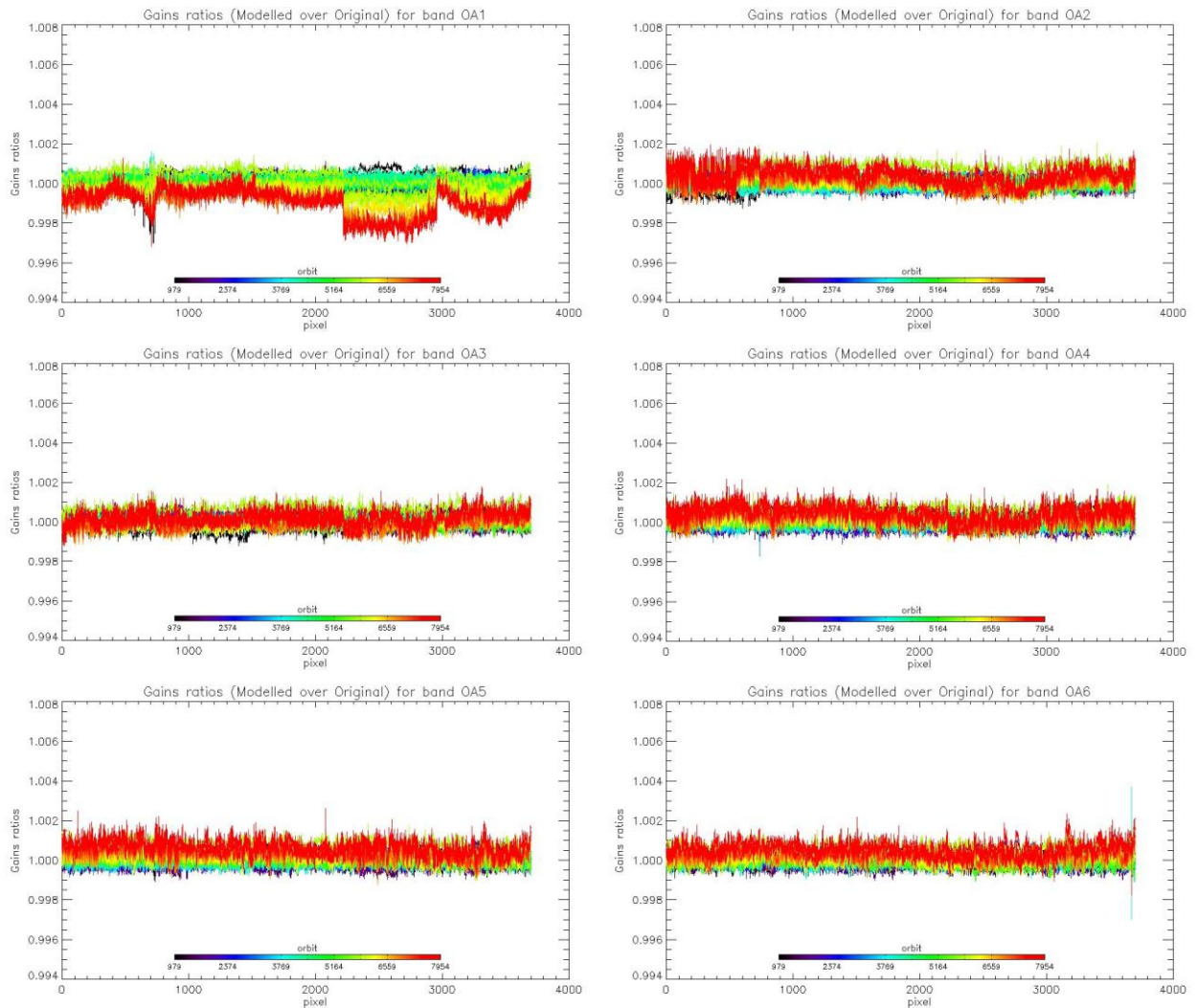


Figure 15: Evolution model performance, as ratio of Model over Data vs. pixels, all cameras side by side, over the whole current calibration dataset (since instrument programming update), including 8 calibration in extrapolation, channels Oa1 to Oa6.



Sentinel-3 MPC
S3-A OLCI Cyclic Performance Report
Cycle No. 021

Ref.: S3MPC.ACR.PR.01-021
Issue: 1.0
Date: 08/09/2017
Page: 14

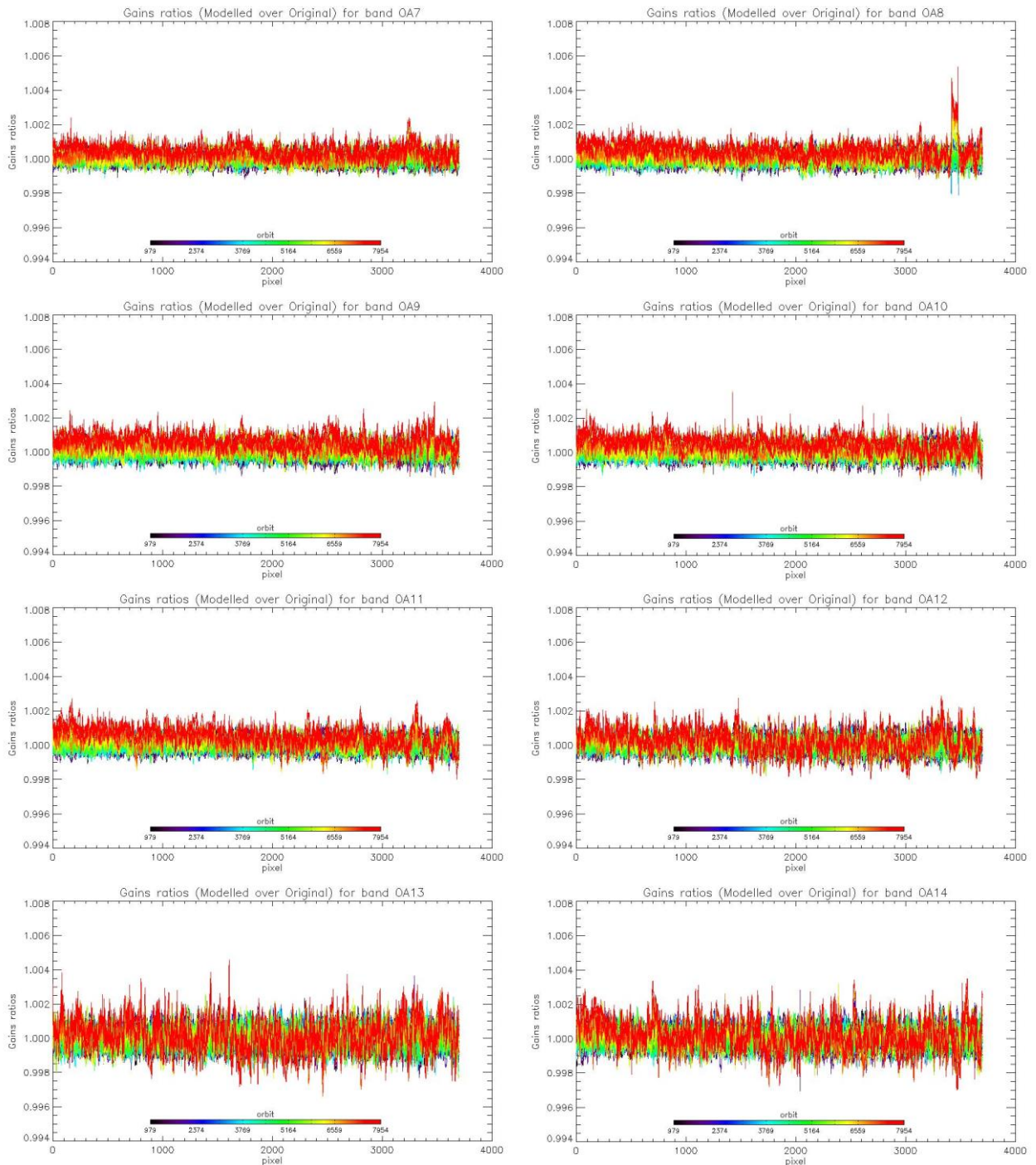


Figure 16: same as Figure 14 for channels Oa7 to Oa14.



Sentinel-3 MPC
S3-A OLCI Cyclic Performance Report
Cycle No. 021

Ref.: S3MPC.ACR.PR.01-021
Issue: 1.0
Date: 08/09/2017
Page: 15

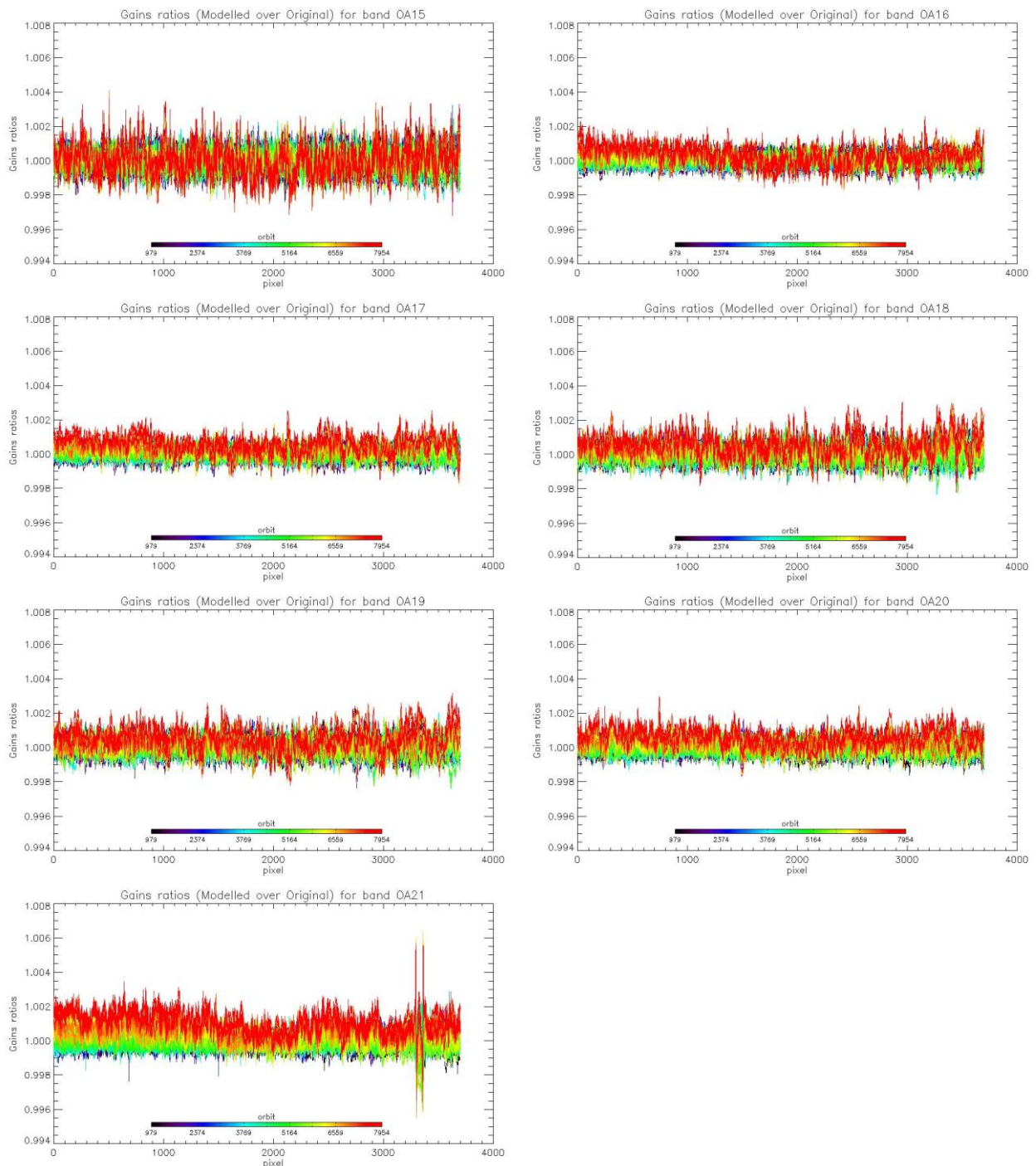


Figure 17: same as Figure 15 for channels Oa15 to Oa21.

1.2.3 Ageing of nominal diffuser [OLCI-L1B-CV-240]

There has been no calibration sequence S05 (reference diffuser) acquisition during cycle 021.

Consequently the last updated results (cycle 020) are still valid

	Sentinel-3 MPC S3-A OLCI Cyclic Performance Report Cycle No. 021	Ref.: S3MPC.ACR.PR.01-021 Issue: 1.0 Date: 08/09/2017 Page: 16
--	---	---

1.2.4 Updating of calibration ADF [OLCI-L1B-CV-260]

A new calibration ADF has been generated, taking the opportunity of a Processing Baseline delivery, to refresh the Dark Correction tables with recent data (22/07). All other parameters remain identical to the current PB. This ADF is the first one benefiting from HEP filtering (see above).

S3A_OL_1_CAL_AX_20170722T080911_20991231T235959_20170904T120000_____MPC_O_AL_016.SEN3

Note: if the final version of the product has been generated after the end of Cycle 21, most of the work necessary for its generation took place during the Cycle, reason why it is mentioned here.

1.2.5 Radiometric Calibrations for sun azimuth angle dependency and Yaw Manoeuvres for Solar Diffuser on-orbit re-characterization [OLCI-L1B-CV-270 and OLCI-L1B-CV-280]

This activity has not evolved during cycle 021 and results presented in previous report are still valid.

1.3 Spectral Calibration [OLCI-L1B-CV-400]

There has been no Spectral Calibration acquisitions sequence S02/S03 during cycle 021.

Consequently the last updated results (cycle 018) are still valid.

1.4 Signal to Noise assessment [OLCI-L1B-CV-620]

1.4.1 SNR from Radiometric calibration data.

SNR computed for all calibration data as a function of band number is presented in Figure 18.

SNR computed for all calibration data as a function of orbit number for band Oa01 (the less stable band) is presented in Figure 19.

There is no significant evolution of this parameter during the current cycle and the ESA requirement is fulfilled for all bands.

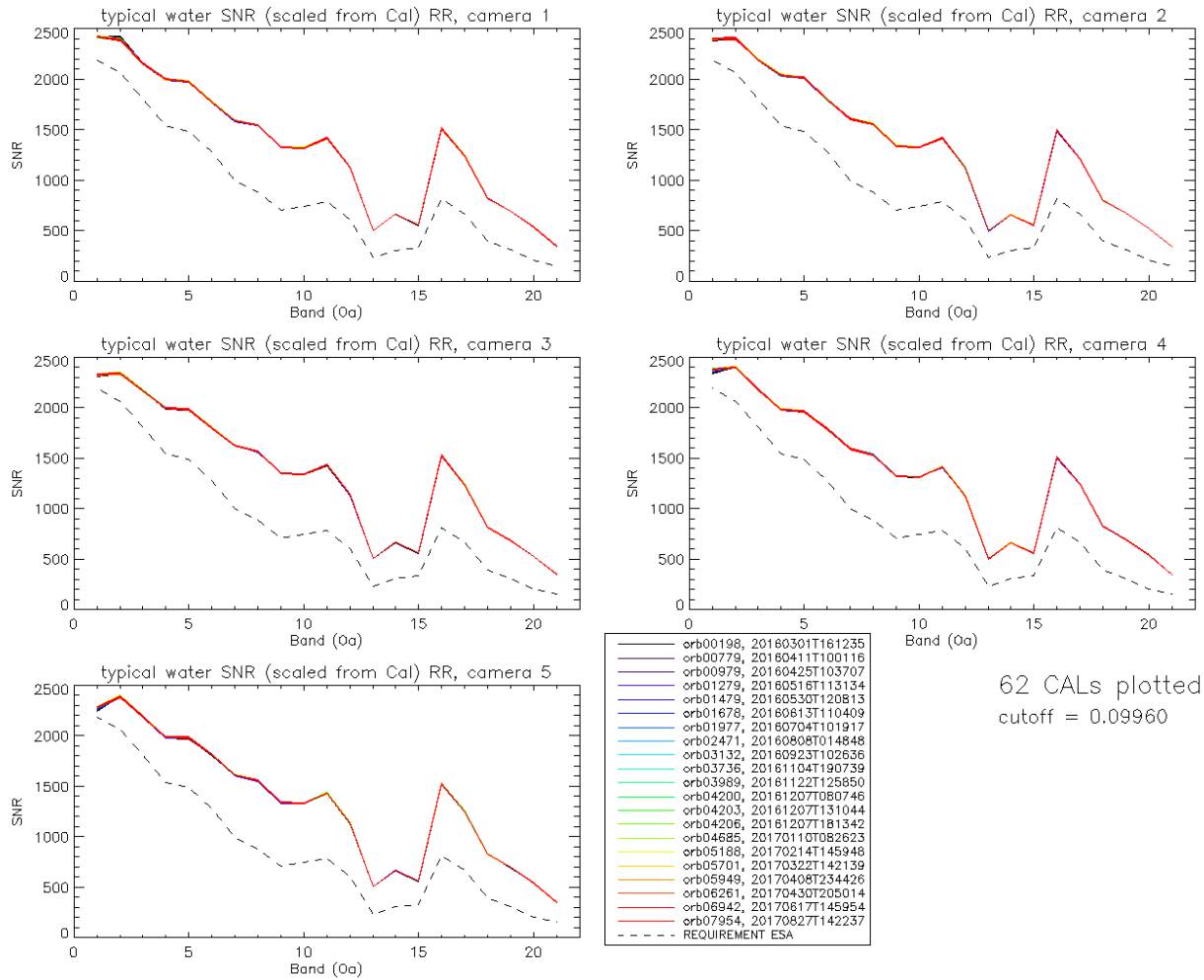


Figure 18: Signal to Noise ratio as a function of the spectral band for the 5 cameras. These results have been computed from radiometric calibration data. All calibrations except first one (orbit 183) are presents with the colours corresponding to the orbit number (see legend). The SNR is very stable with time: the curves for all orbits are almost superimposed. The dashed curve is the ESA requirement.

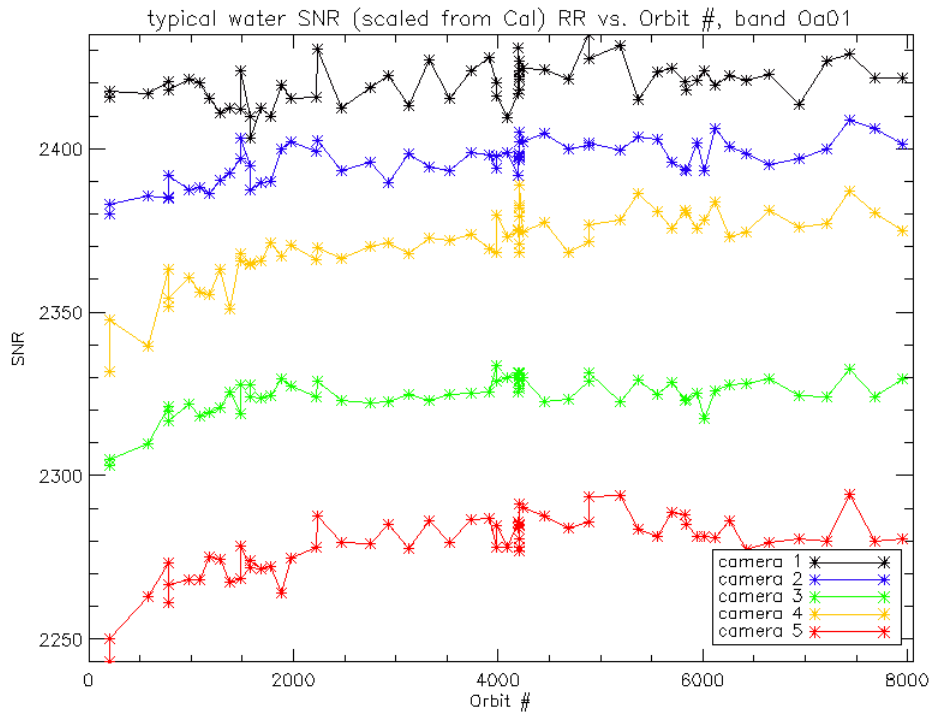


Figure 19: long-term stability of the SNR estimates from Calibration data, example of channel Oa01.

The mission averaged SNR figures are provided in Table 1 below, together with their radiance reference level. According to the OLCI SNR requirements, these figures are valid at these radiance levels and at Reduced Resolution (RR, 1.2 km). They can be scaled to other radiance levels assuming shot noise (CCD sensor noise) is the dominating term, i.e. radiometric noise can be considered Gaussian with its standard deviation varying as the square root of the signal; in other words: $SNR(L) = SNR(L_{ref}) \cdot \sqrt{\frac{L}{L_{ref}}}$. Following the same assumption, values at Full Resolution (300m) can be derived from RR ones as 4 times smaller.



Sentinel-3 MPC
S3-A OLCI Cyclic Performance Report
Cycle No. 021

Ref.: S3MPC.ACR.PR.01-021
 Issue: 1.0
 Date: 08/09/2017
 Page: 19

Table 1: SNR figures as derived from Radiometric Calibration data. Figures are given for each camera (time average and standard deviation), and for the whole instrument. The requirement and its reference radiance level are recalled (in $mW.sr^{-1}.m^{-2}.nm^{-1}$).

λ nm	L_{ref} LU	SNR RQT	C1		C2		C3		C4		C5		All	
			avg	std										
400	63	2188	2420	6.5	2396	6.2	2324	6	2370	11	2278	10	2357	6.5
412.5	74.1	2061	2396	8.3	2409	5.4	2340	4.7	2402	4.5	2386	7.3	2387	4.2
442.5	65.6	1811	2161	5.4	2199	5.8	2167	4.5	2185	4.3	2197	4.9	2182	3.4
490	51.2	1541	1999	5	2035	5.4	1995	3.6	1981	4	1987	5.2	1999	3.6
510	44.4	1488	1979	5.5	2012	5	1982	4.9	1965	4.5	1984	5	1984	3.9
560	31.5	1280	1775	4.4	1801	4.4	1801	4.9	1793	4	1817	3.8	1798	3.3
620	21.1	997	1591	4.2	1609	4.2	1625	3.4	1593	3.6	1614	3.7	1606	2.8
665	16.4	883	1546	4.7	1558	4.2	1566	3.7	1532	4.4	1560	3.9	1552	3.3
673.75	15.7	707	1329	3.4	1337	4	1350	2.9	1323	3.1	1341	4	1336	2.7
681.25	15.1	745	1319	3.7	1326	3.2	1337	3.1	1314	2.5	1332	3.9	1326	2.3
708.75	12.7	785	1420	4.6	1420	4.4	1434	3.7	1413	3.9	1429	3.1	1423	3.2
753.75	10.3	605	1126	3.5	1119	3.4	1133	3.9	1123	2.7	1138	3	1128	2.8
761.25	6.1	232	501	1.3	498	1.5	504	1.4	500	1.2	507	1.5	502	1.1
764.375	7.1	305	662	1.8	657	1.7	667	2.4	660	1.8	668	2.1	663	1.6
767.5	7.6	330	558	1.8	554	1.3	561	1.6	556	1.8	563	1.5	558	1.4
778.75	9.2	812	1513	5.4	1496	5.4	1522	5.6	1509	5.6	1524	5.2	1513	4.8
865	6.2	666	1243	3.8	1212	4.4	1237	4.4	1245	3.9	1249	3	1237	3.4
885	6	395	823	1.9	801	1.8	813	2.1	824	1.6	830	2	818	1.4
900	4.7	308	691	1.6	673	1.4	682	1.8	692	1.5	697	1.5	687	1.1
940	2.4	203	534	1.1	522	1.2	525	1.1	539	1.2	541	1.2	532	0.8
1020	3.9	152	345	0.8	337	0.7	348	0.7	345	0.8	351	0.7	345	0.5

1.4.2 SNR from EO data.

There has been no update on SNR assessment from EO data during the cycle. Last figures (cycle 9) are considered valid.

1.5 Geometric Calibration/Validation

Regular monitoring using the GeoCal Tool implemented within the MPMF continues. Late August results confirm good performance. Monitoring of the geolocation performance by correlation with GCP imageries using the GeoCal tool over the period confirms that OLCI is compliant with its requirement: the centroid of the geolocation error is around 0.25 pixel in both along-track and across-track directions (Figure 20 & Figure 21). The dispersion of the along-track errors in Figure 21 suggests however that a

per-camera analysis is required. Completion of the time series (started using the partial reprocessing dedicated to validation: 4 days every month between 26/04/16 and 12/03/2017) confirms the slow AL trend (Figure 22).

Performing additional geometric Calibration has to be done in a near future. This requires however using the GeoCal tool in Calibration mode, a mode that is not available in the GeoCal tool version implemented in the MPMF. Discussion has been started with ESTEC to see if their support can be envisaged.

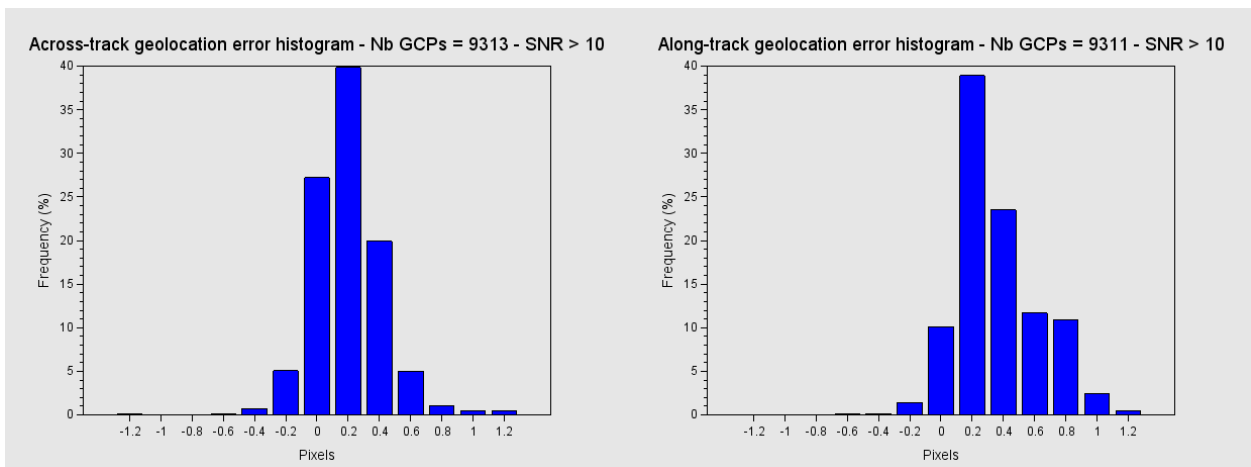


Figure 20: histograms of geolocation errors for the along-track (left) and across-track (right) directions, example 20/08/2017.

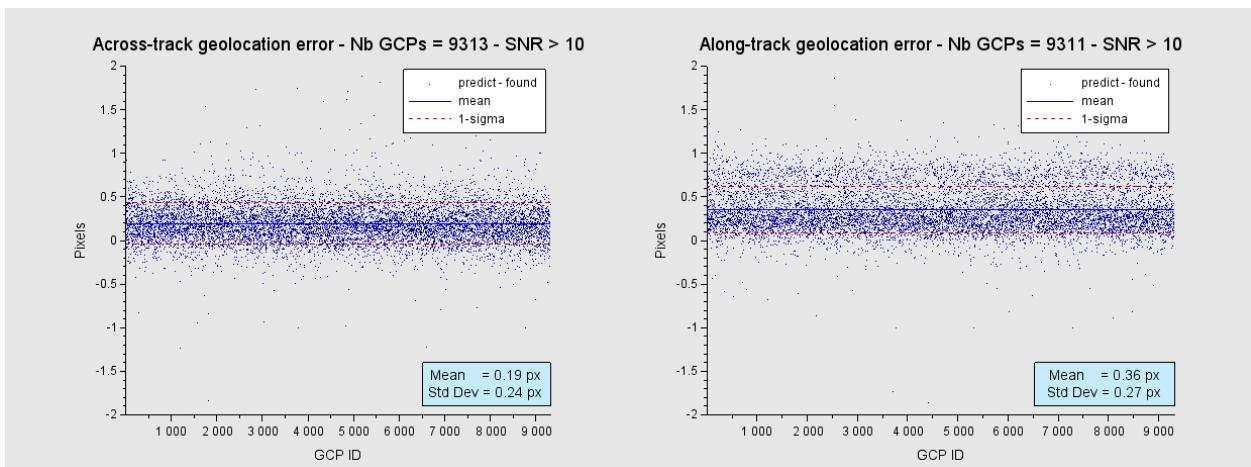


Figure 21: georeferencing error in along-track (left) and across-track (right) directions for all the GCPs, example of 20/08/2017.



Sentinel-3 MPC
S3-A OLCI Cyclic Performance Report
Cycle No. 021

Ref.: S3MPC.ACR.PR.01-021
Issue: 1.0
Date: 08/09/2017
Page: 21

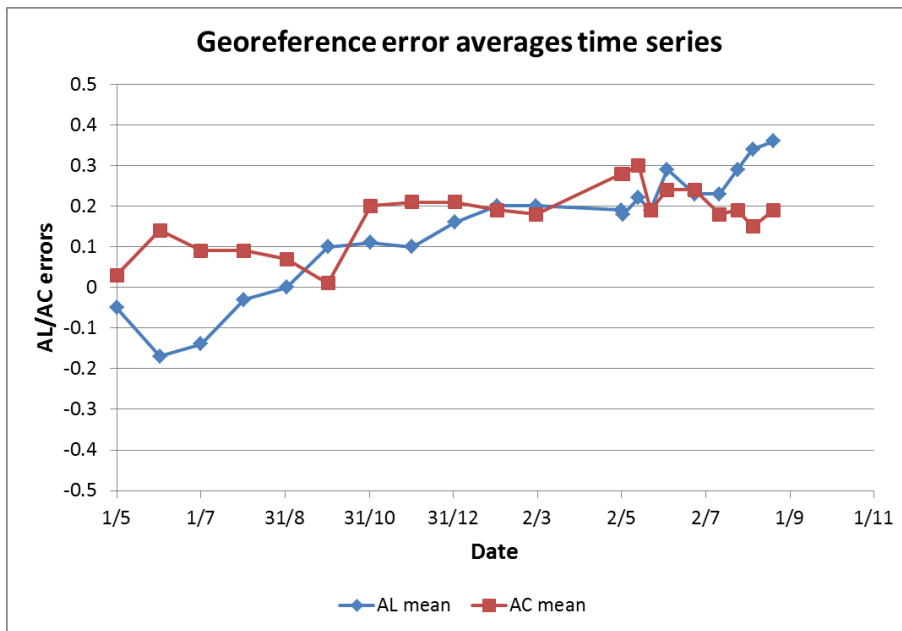


Figure 22: time series of geolocation errors for the along-track (blue) and across-track (red) directions over 15.6 months.

	Sentinel-3 MPC S3-A OLCI Cyclic Performance Report Cycle No. 021	Ref.: S3MPC.ACR.PR.01-021 Issue: 1.0 Date: 08/09/2017 Page: 22
--	---	---

2 OLCI Level 1 Product validation

2.1 [OLCI-L1B-CV-300], [OLCI-L1B-CV-310] – Radiometric Validation

2.1.1 S3ETRAC Service

Activities done

The S3ETRAC service extracts OLCI L1 RR and SLSTR L1 RBT data and computes associated statistics over 49 sites corresponding to different surface types (desert, snow, ocean maximizing Rayleigh signal, ocean maximizing sunglint scattering and deep convective clouds). The S3ETRAC products are used for the assessment and monitoring of the L1 radiometry (optical channels) by the ESLs.

All details about the S3ETRAC/OLCI and S3ETRAC/SLSTR statistics are provided on the S3ETRAC website <http://s3etrac.acri.fr/index.php?action=generalstatistics>

- ❖ Number of OLCI products processed by the S3ETRAC service
- ❖ Statistics per type of target (DESERT, SNOW, RAYLEIGH, SUNGLINT and DCC)
- ❖ Statistics per sites
- ❖ Statistics on the number of records

For illustration, we provide below statistics on the number of S3ETRAC/OLCI records generated per type of targets (DESERT, SNOW, RAYLEIGH, SUNGLINT and DCC).

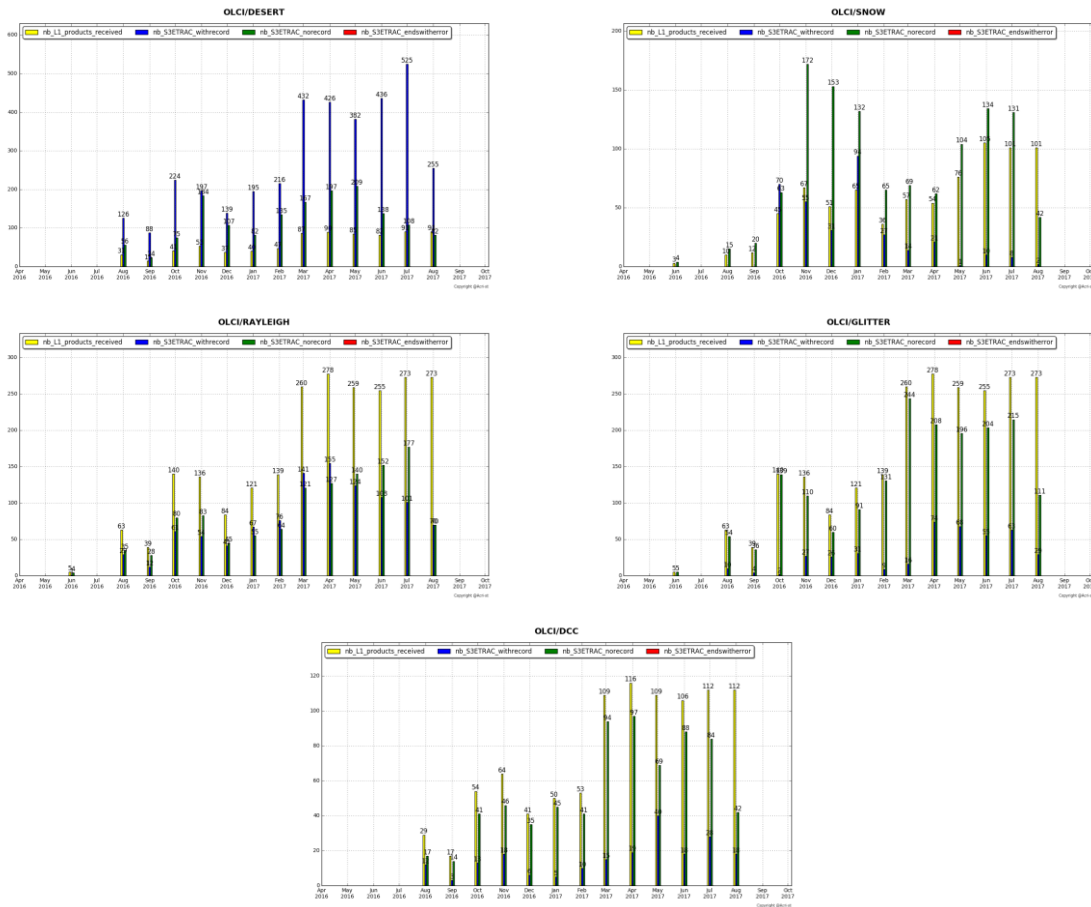


Figure 23: summary of S3ETRAC products generation for OLCI (number of OLCI L1 products Ingested, yellow – number of S3ETRAC extracted products generated, blue – number of S3ETRAC runs without generation of output product (data not meeting selection requirements), green – number of runs ending in error, red, one plot per site type).

2.1.2 Radiometric validation with DIMITRI

Highlights

- ❖ Run Desert and Rayleigh method over the available products until 5th September*.
- ❖ Run Desert and Glint method over the available products until 18th August.
- ❖ The results are consistent with the previous ones (Rayleigh, Glint and PICS).
- ❖ Rather good stability of the sensor could be seen, nevertheless, the time-series average shows higher reflectance over the VNIR spectral range with bias of 3%-5% except bands Oa07-Oa09; bands with high gaseous absorption are excluded.
- ❖ The results are consistent over the used CalVal sites
- ❖ The results need to be consolidated over ocean sites with more products from early mission period.



I-Validation over PICS

1. Downloading and ingestion of all the available L1B-LN1-NT products in the S3A-Opt database over the 6 desert calval-sites (Algeria3 & 5, Libya 1 & 4 and Mauritania 1 & 2) is on-going. The ingested time-series has been extended until 18th August 2017. Note that only few products over the 6 PICS were found during Cycle-21 period due to an issue with the mini-file generation (see SIIIMPC-1796).
2. The results are consistent overall the six used PICS sites (Figure 24). OLCI reflectance shows rather good stability over the mission life-time.
3. The temporal average over the period **April 2016 – September 2017** of the elementary ratios (observed reflectance to the simulated one) shows values higher than 2% (mission requirements) over all the VNIR bands (Figure 25). The spectral bands with significant absorption from water vapour and O₂ (Oa11, Oa13 and Oa14) show an outlier ratio.

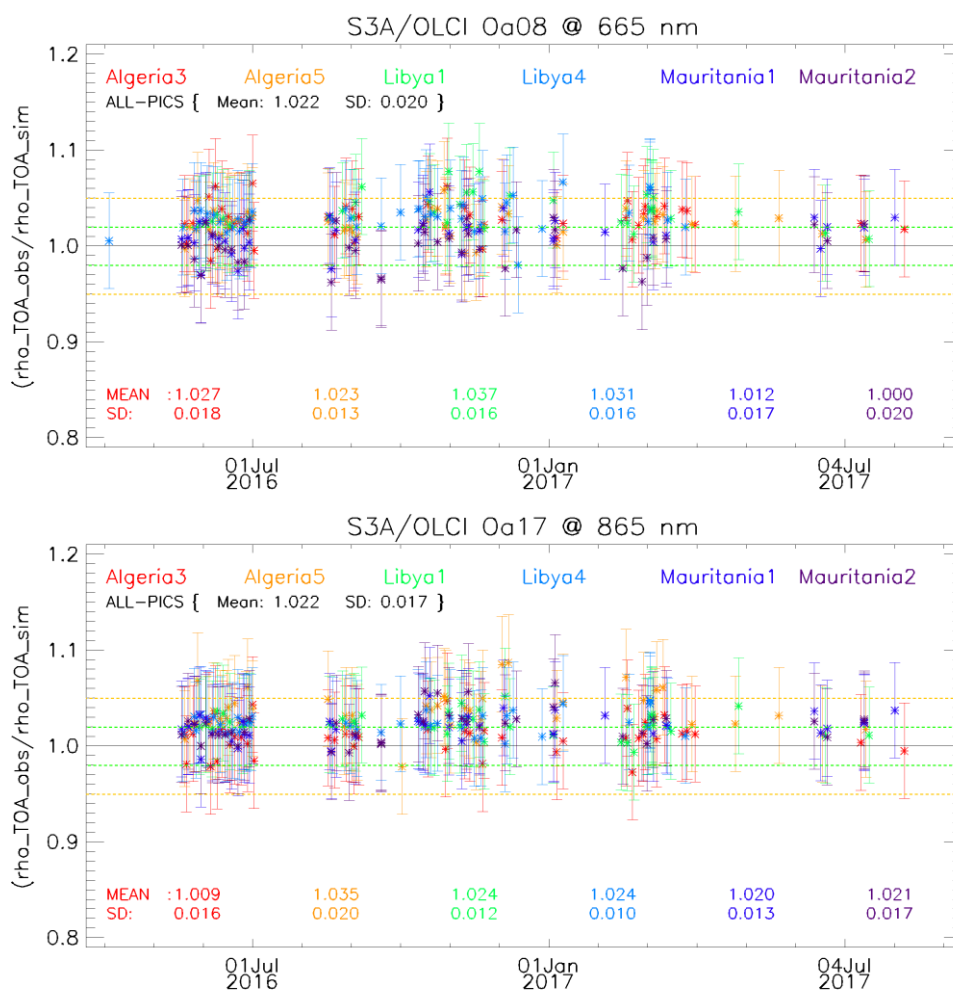


Figure 24: Time-series of the elementary ratios (observed/simulated) signal from S3A/OLCI for (top to bottom) bands Oa03, Oa8 and Oa17 respectively over Six PICS Cal/Val sites. Dashed-green and orange lines indicate the 2% and 5% respectively. Error bars indicate the desert methodology uncertainty.

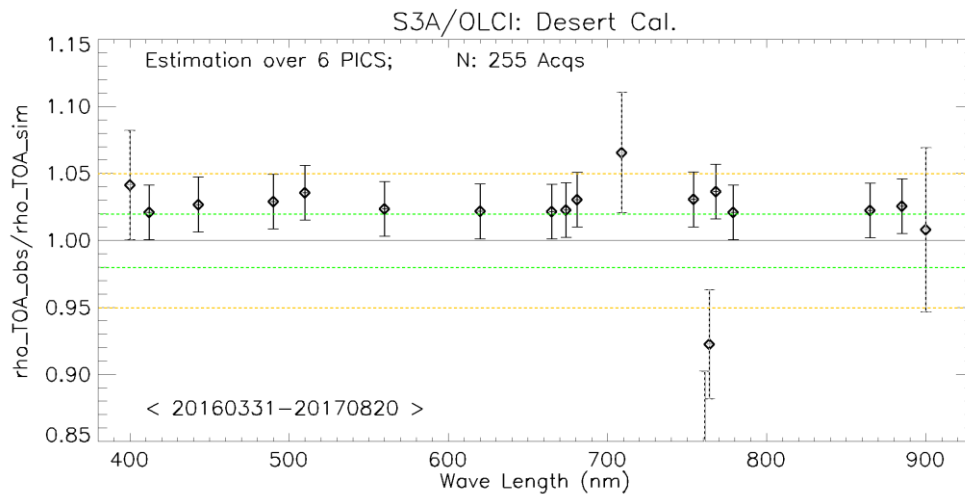


Figure 25: The estimated gain values for S3A/OLCI over the 6 PICS sites identified by CEOS over the period April 2016 – July 2017 as a function of wavelength. Dashed-green and orange lines indicate the 2% and 5% respectively. Error bars indicate the desert methodology uncertainty.

II-Intercomparison S3A/OLCI, S2A/MSI and LANDSAT/OLI over PICS

1. X-mission Intercomparison with MSI-A and MODIS-A is performed until August 2017. Figure 26 shows time-series of the elementary ratios from S2A/MSI, Aqua/MODIS and S3A/OLCI over ALGERIA5 and LIBYA1 over the period March-2016 until August-2017.

We observe a clear stability over the three sensors, associated with high reflectance from OLCI wrt to MSI and MODIS ones.

Figure 27 shows the estimated gain over the different time-series from different sensors (MODISA, MSIA, MSIB, OLCI and OLI) compared to the estimated gain over MERIS 3rd RP over PICS, for the common bands between S2A/MSI, Aqua/MODIS and S3A/OLCI over ALGERIA5 and LIBYA1. Again Figure 27 confirms a systematic higher reflectance of OLCI wrt MSI and MODISA.

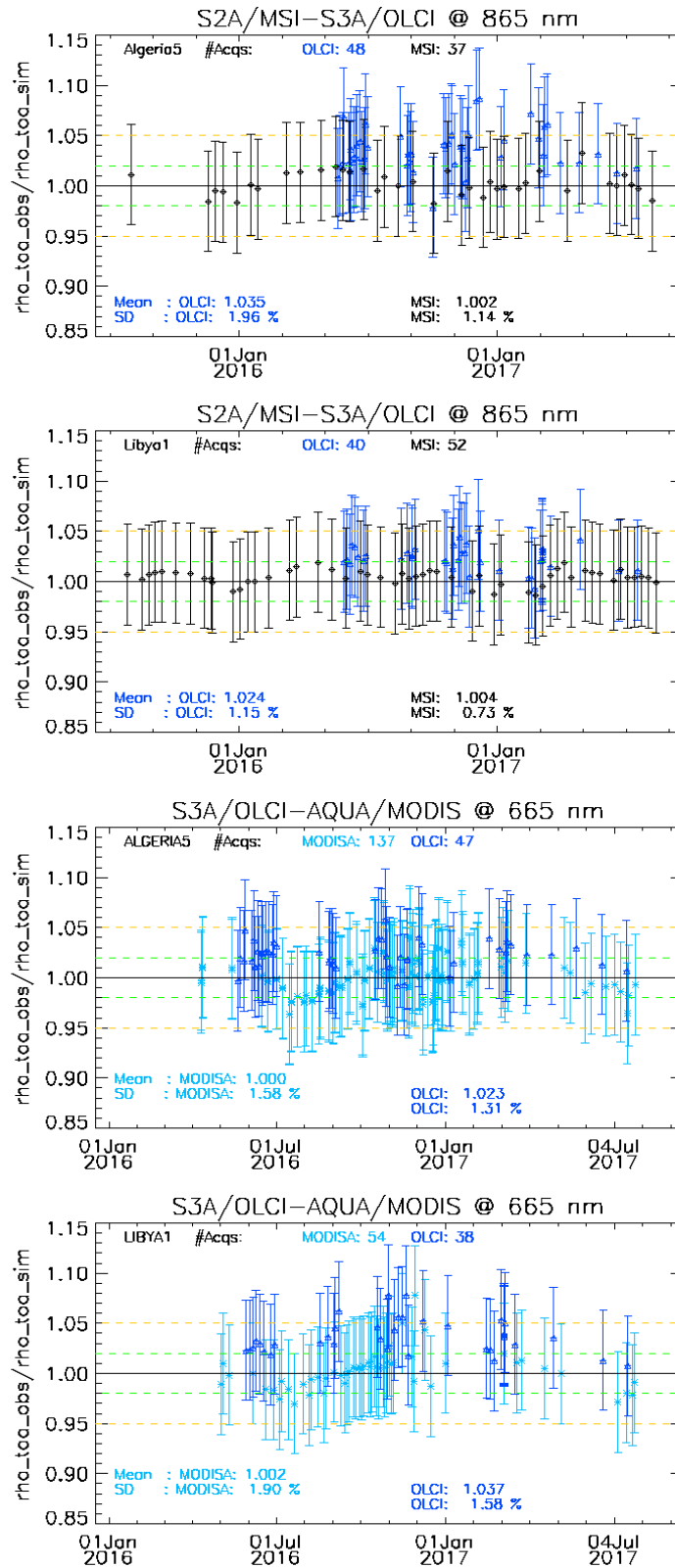


Figure 26: Time-series of the elementary ratios (observed/simulated) signal from (black) S2A/MSI, (blue) S3A/OLCI and (Cyan) Aqua/MODIS for (band Oa17: 865nm and Oa08: 665 nm over ALGERIAS5 and LIBYA1 sites. Dashed-green and orange lines indicate the 2% and 5% respectively. Error bars indicate the desert methodology uncertainty.

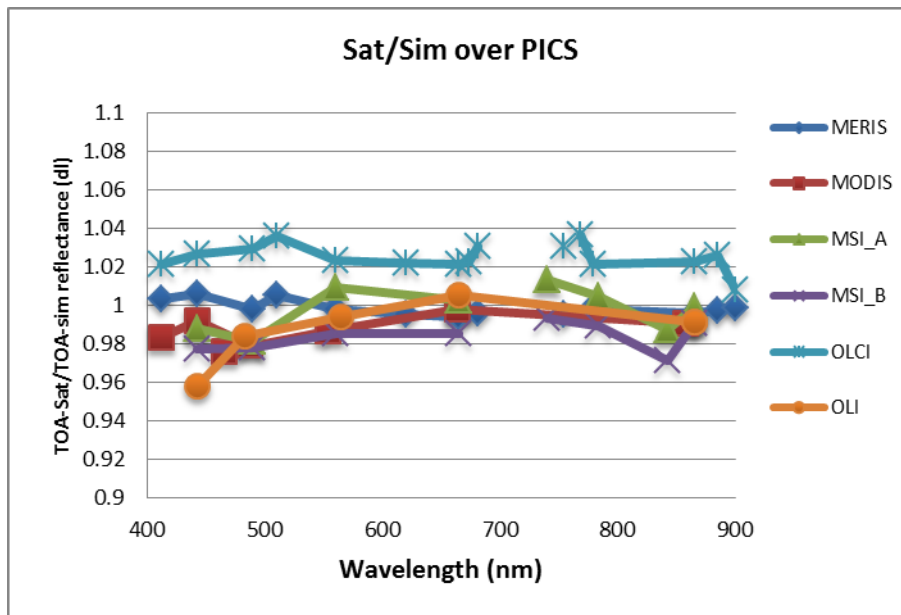


Figure 27: The estimated gain values (observed-signal /simulated-signal) averaged over different period from different sensors over PICS as function of wavelength.

III-Validation over Rayleigh

Rayleigh method has been performed over the available mini-files on the Opt-server until the cycle-21 period. The results produced with the configuration (ROI-AVERAGE) are consistent with the previous results of PICS method and from Cycle-20. While bands Oa01-Oa05 display a bias values between 2%-5%, bands Oa6-Oa9 exhibit biases within 2% (mission requirements) (Figure 28).

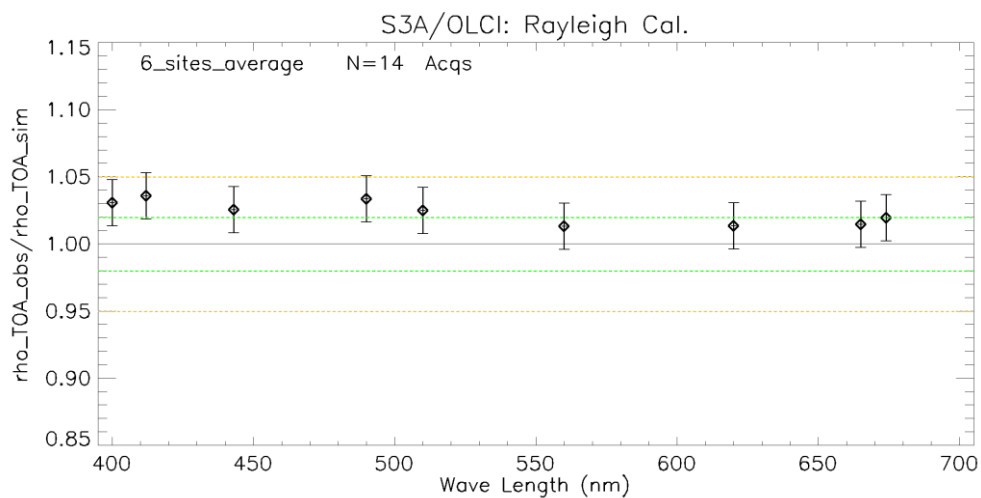


Figure 28: The estimated gain values for S3A/OLCI over the 6 Ocean CalVal sites (Atl-NW_Optimum, Atl-SW_Optimum, Pac-NE_Optimum, Pac-NW_Optimum, SPG_Optimum and SIO_Optimum) over the period December 2016 – September 2017 as a function of wavelength. Dashed-green, and orange lines indicate the 2%, 5% respectively. Error bars indicate the methodology uncertainty.



IV-Validation over Glint

This section is not updated, as the Glint method was not performed over Cycle-21.

Glint calibration method with the configuration (ROI-PIXEL) has been performed over the period December 2016 – end June 2017 from the available mini-files. The outcome of this analysis shows a good consistency with Rayleigh and the desert outputs over the NIR spectral range (see Figure-29).

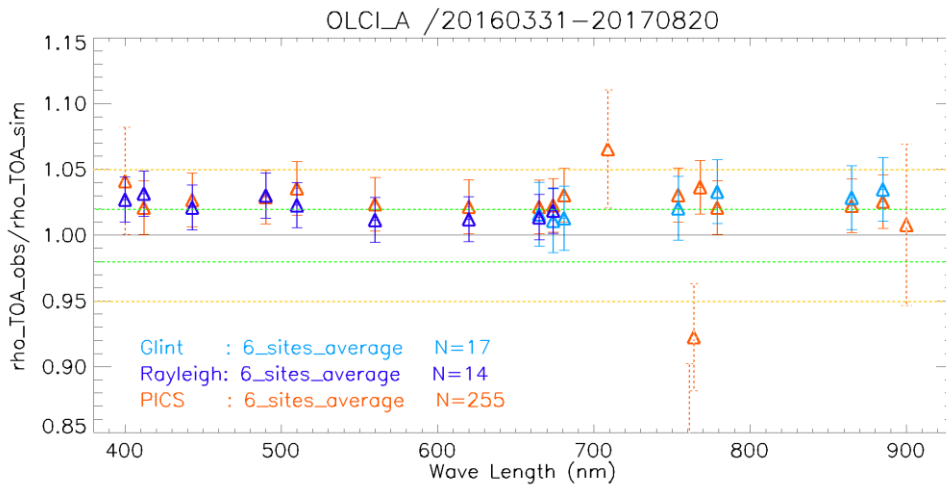


Figure-29 : The estimated gain values for S3A/OLCI from Glint, Rayleigh, and PICS over the period March 2016 – August 2017 for PICS and December 2016-September 2017 for Rayleigh and December 2016-July 2017 Glint methods as a function of wavelength. We use the gain value of Oa8 from PICS method as reference gain for Glint. Dashed-green and orange lines indicate the 2% and 5% respectively. Error bars indicate the methods uncertainties.

2.1.3 Radiometric validation with OSCAR

The S3ETRAC Rayleigh scenes from May to June 2017 have been processed with OSCAR. Corresponding average Rayleigh results per site are given in Figure 30. The obtained Rayleigh results for band 1 (at 400 nm) should however be considered with care due to larger uncertainty in the radiative transfer calculations.

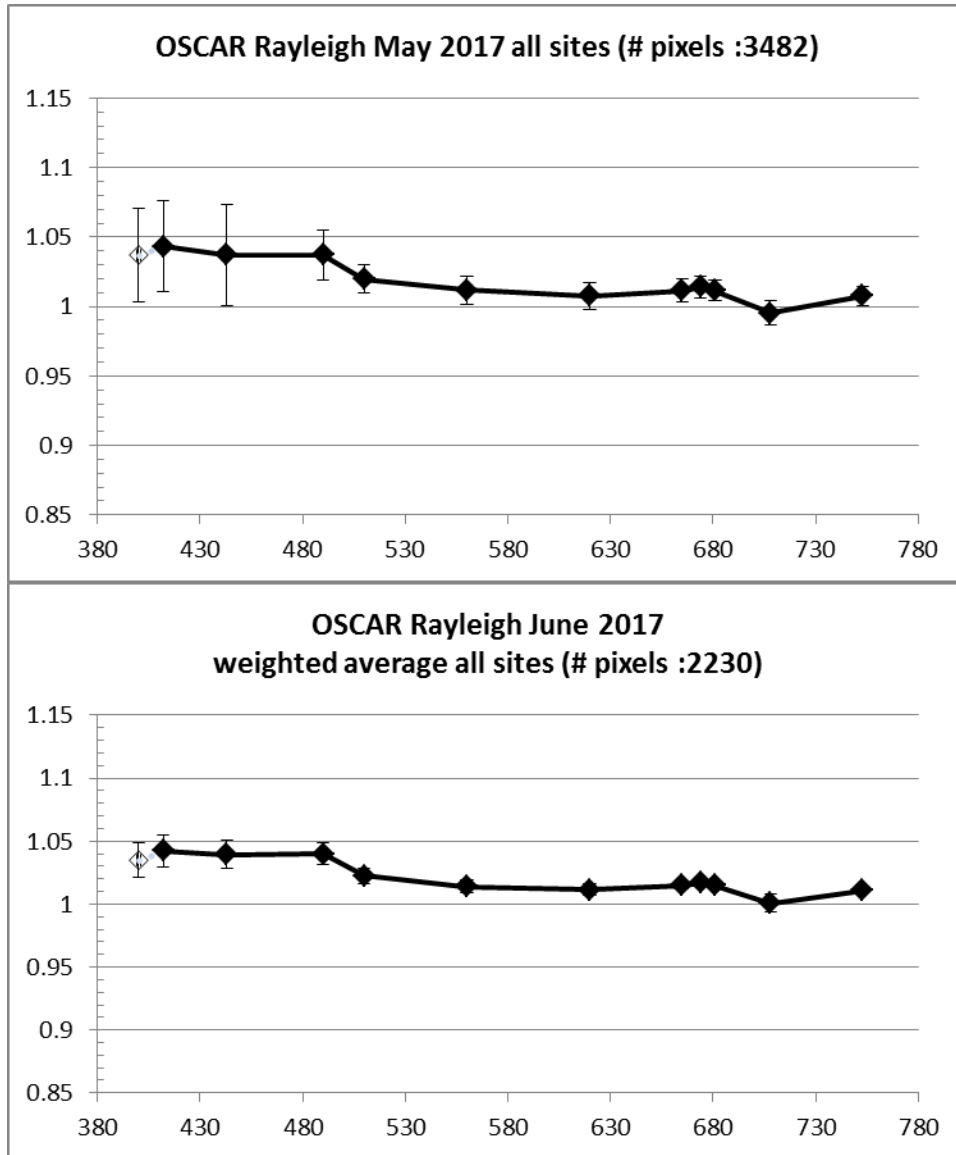


Figure 30: OSCAR Rayleigh results for May and June 2017.

2.2 [OLCI-L1B-CV-320] – Radiometric Validation with Level 3 products

There has been no new result during the cycle. Last figures (cycle 20) are considered valid

	Sentinel-3 MPC S3-A OLCI Cyclic Performance Report Cycle No. 021	Ref.: S3MPC.ACR.PR.01-021 Issue: 1.0 Date: 08/09/2017 Page: 30
--	---	---

3 Level 2 Land products validation

3.1 [OLCI-L2LRF-CV-300]

All routine extractions and statistics have been generated nominally over for the reporting period, within the limitations imposed by the data availability issues. However, there has been no update on Land products validation quantitative assessment during the cycle. Last figures (cycle 18) are considered valid.

Qualitative assessment by product inspection showed no detectable performance evolution.

On the other hand, two specific activities strongly related to Land Products validation took place:

- ❖ Generation of global monthly OTCI composites for promotion:
 - animated L3 products have been delivered to ESA and published at ([http://www.esa.int/Our Activities/Observing the Earth/Copernicus/Sentinel-3/See our seasons change from space](http://www.esa.int/Our_Activities/Observing_the_Earth/Copernicus/Sentinel-3/See_our_seasons_change_from_space))
- ❖ Dedicated in-situ validation data acquisition campaigns have been conducted in July (UoS):

Field validation Campaigns to support OLCI land product validation

Two field validation campaigns were conducted during June-August 2017 to collect in-situ and Airborne data to validate OLCI land products. The fieldwork campaign aimed to collect data about the biophysical variables of FAPAR, LAI and leaf chlorophyll concentration to validate the FAPAR and chlorophyll product from OLCI.

1. Valencia Fieldwork Campaign

This fieldwork campaign took place in June 2017, upon the site of the Valencia Anchor Station (39°34'15"N, 1°17'18"W, 813m). The site comprises of vine plantation, fruit trees and coniferous forest. In total, an area of 10 km² was sampled over 5 days with 50 elementary sampling units (ESU) distributed over different vegetation types.

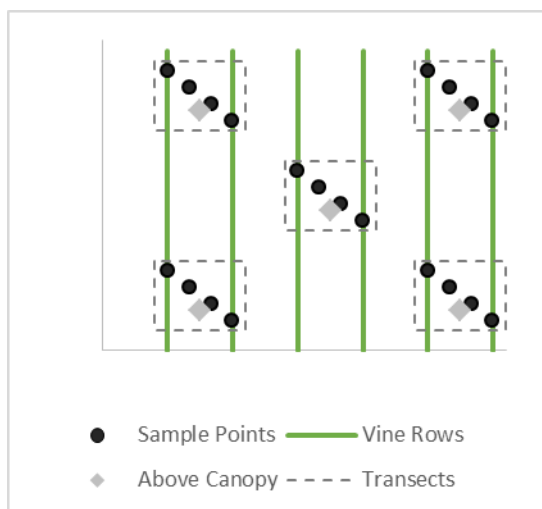


Figure 31 Sampling strategy



Figure 32 False Colour Composition (Band combination: 8,4,3) of the study region, Utiel can be seen in the bottom right corner of the image.

The sampling strategy used within the campaign can be seen above. Each transect covered the distance between one row of vines (1.5m) and moved down the row of vines by two plants (~2m). A similar sampling strategy was used with ESUs of fruit trees, matorral and pine trees. The number of measurements taken within each ESU can be seen within **Table 2**. Four below canopy and one above canopy reading was taken per transect with the LICOR-2200 instrument.

Table 2: Sampling strategy used for the Valencia fieldwork campaign

Technique	Biophysical variable	Number of sampling measures per point	Total number of measurements per ESU
LICOR-2200	LAI	5	25
Spectrometer	Reflectance	2	10
DHP	LAI/FAPAR	4	20
SPAD-502	Chlorophyll	2	30
PAR-sensor	FAPAR	1	25

Estimates of biophysical variables from 26 of the sites have already been processed and the relationships between different vegetation indices and the estimates of biophysical variables derived from Sentinel 2 imagery is currently being examined and evaluated through linear mixing and radiative transfer models.

2. New forest Campaign

The New Forest site (50.8498, -1.5741) comprised of broadleaf deciduous forest with little undergrowth. The dominant species present at the study site are beech (45 %), oak (40 %) and silver birch (5 %). Field data collection was undertaken during August 2017 with simultaneous airborne acquisition. However,

due to bad weather a subset of the planned 10x10km is was covered. In total 25 ESUs were sampled across 4 days.

Future activity over next 6 months:

1. Collate and quality check field data from both campaign
2. Pre-process airborne data
3. Develop upscaling method to produce high resolution biophysical variable maps for both sites
4. Validate OLCI vegetation product
5. Perform radiative transfer modelling to simulate FAPAR for the field site

Routine OLCI Data Extractions over Core Validation Sites, Time Series

The graphs below provide the OLCI FR OGVI and OTCI time series over core validation sites computed on 3x3 macropixels. The OTCI time series remain as expected pretty stable over the summer period. The OGVI time series however can demonstrate significant variation (ITTra, SPALi, SPVal) whatever the macropixel site used. Cloud detection might be considered as the potential source of this variability (Figure 38). On Figure 39 example however, the cloud detection cannot be at the origin of this variability.

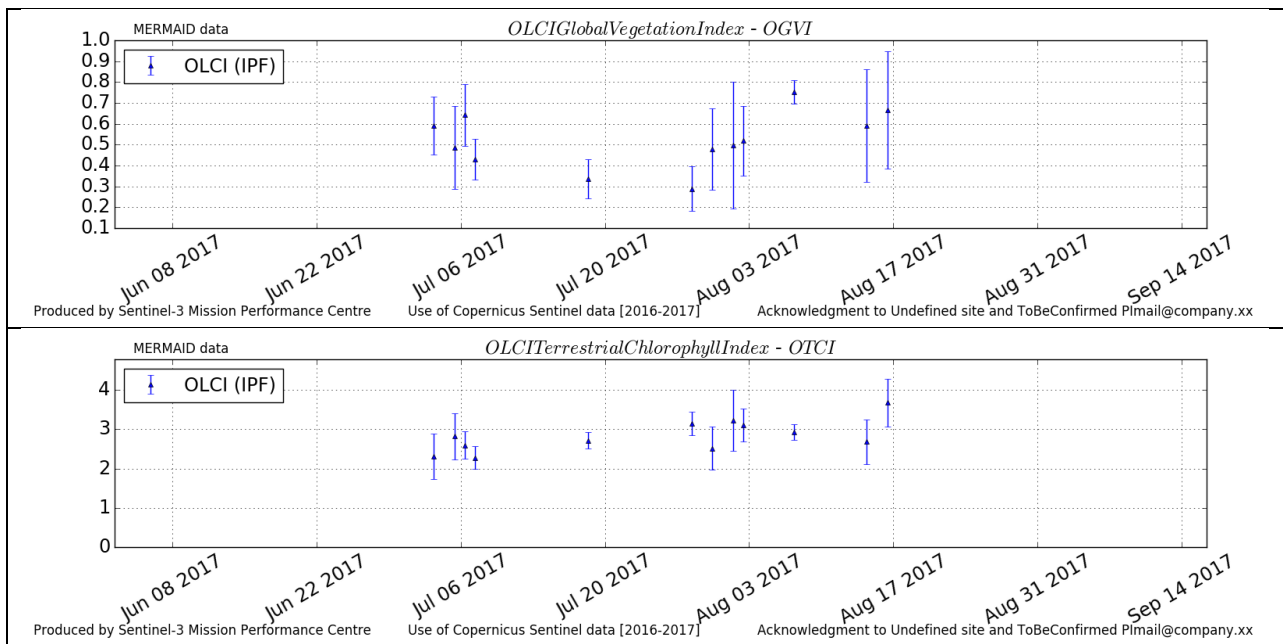


Figure 33: DEGeb time series



Sentinel-3 MPC

S3-A OLCI Cyclic Performance Report

Cycle No. 021

Ref.: S3MPC.ACR.PR.01-021
Issue: 1.0
Date: 08/09/2017
Page: 33

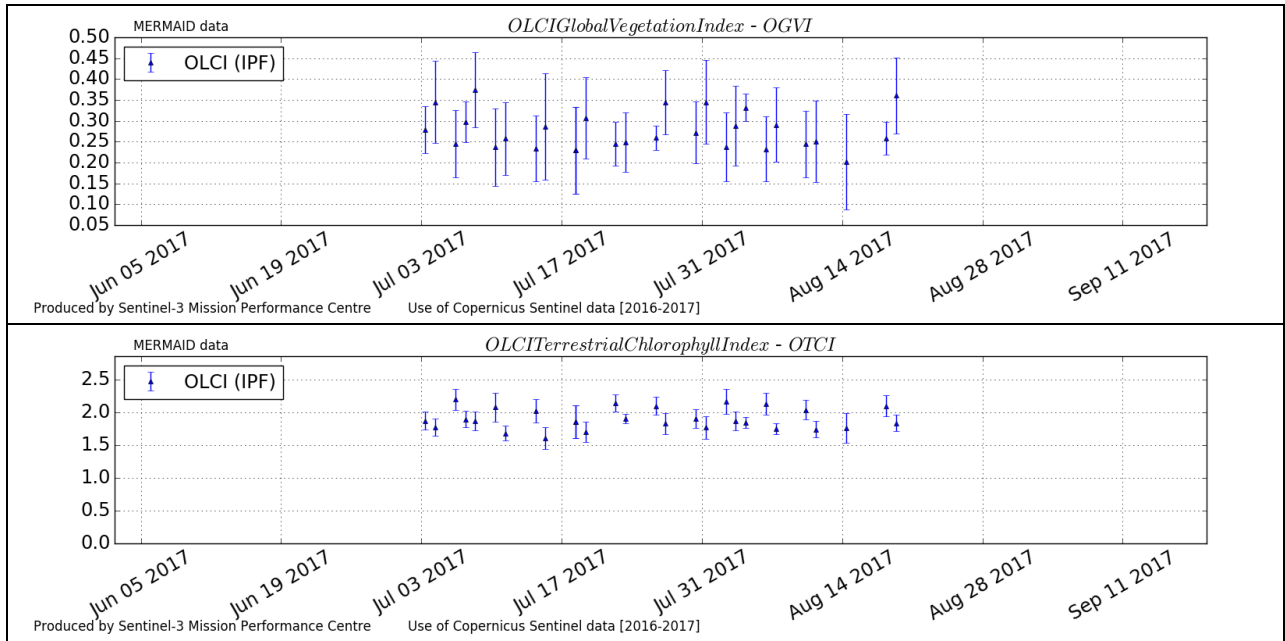


Figure 34: ITCat time series

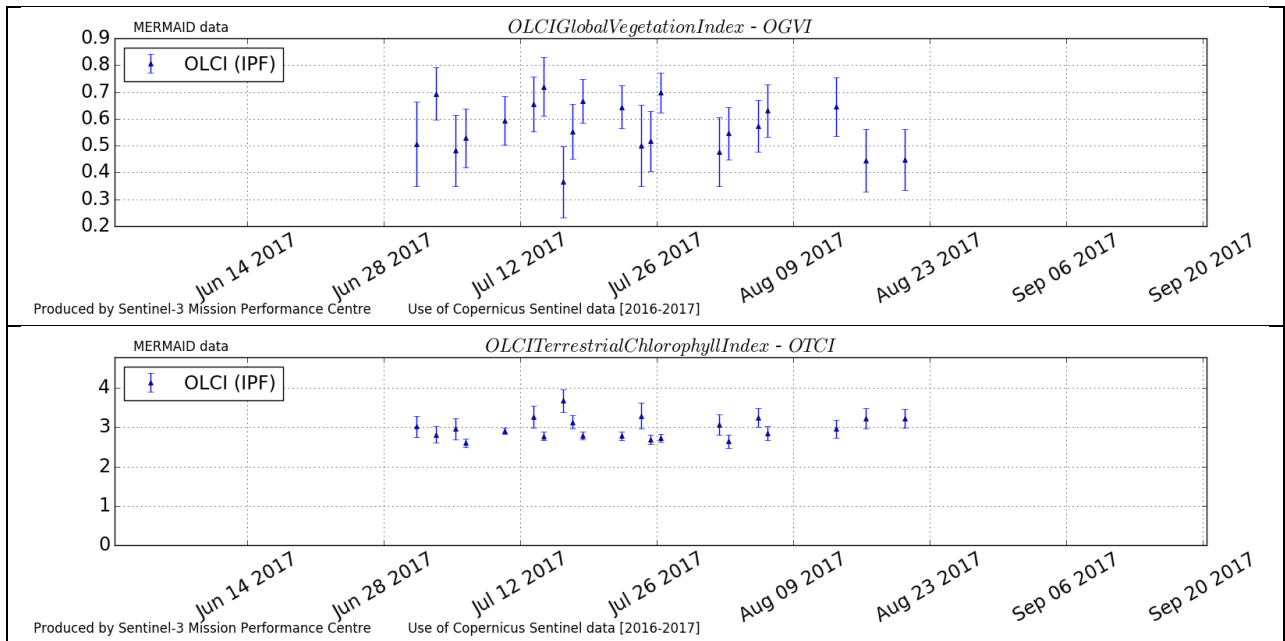


Figure 35: ITIsp time series



Sentinel-3 MPC
S3-A OLCI Cyclic Performance Report
Cycle No. 021

Ref.: S3MPC.ACR.PR.01-021
Issue: 1.0
Date: 08/09/2017
Page: 34

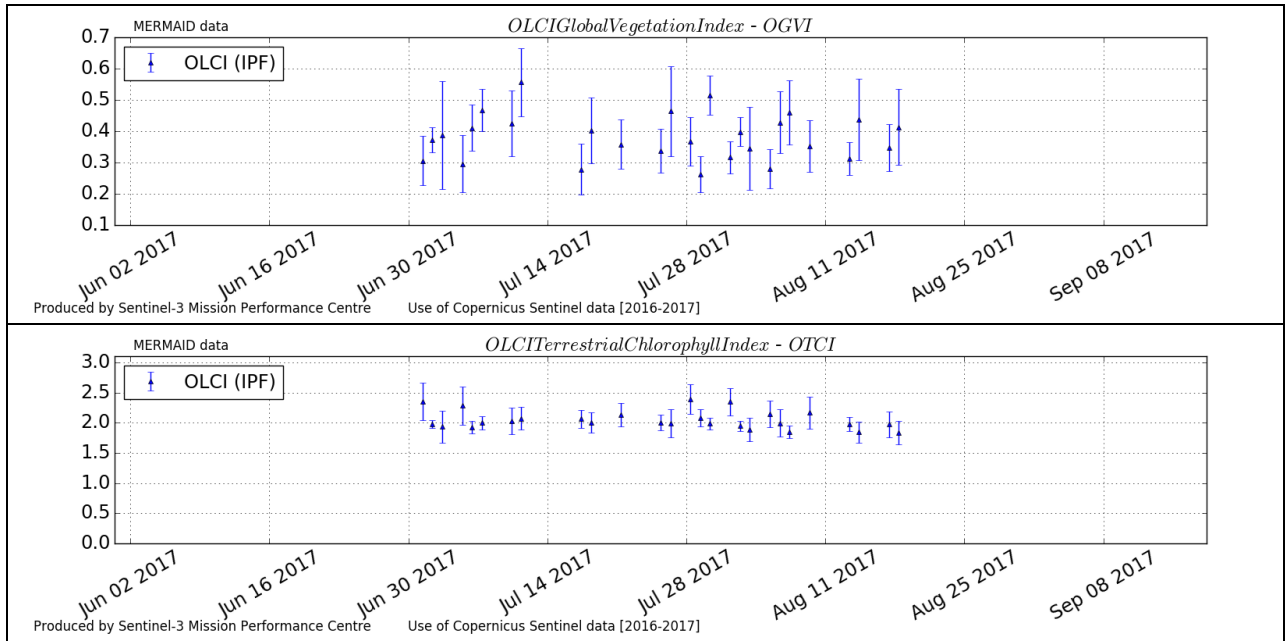


Figure 36: ITSro time series

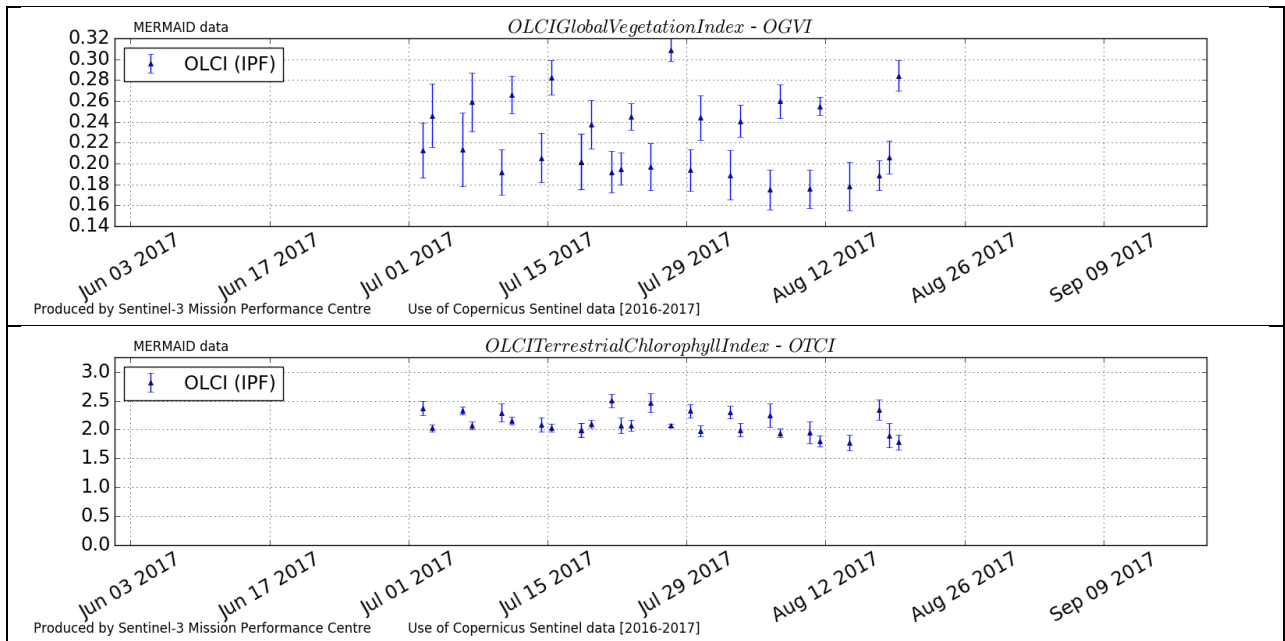


Figure 37: ITTra time series



Sentinel-3 MPC
S3-A OLCI Cyclic Performance Report
Cycle No. 021

Ref.: S3MPC.ACR.PR.01-021
 Issue: 1.0
 Date: 08/09/2017
 Page: 35

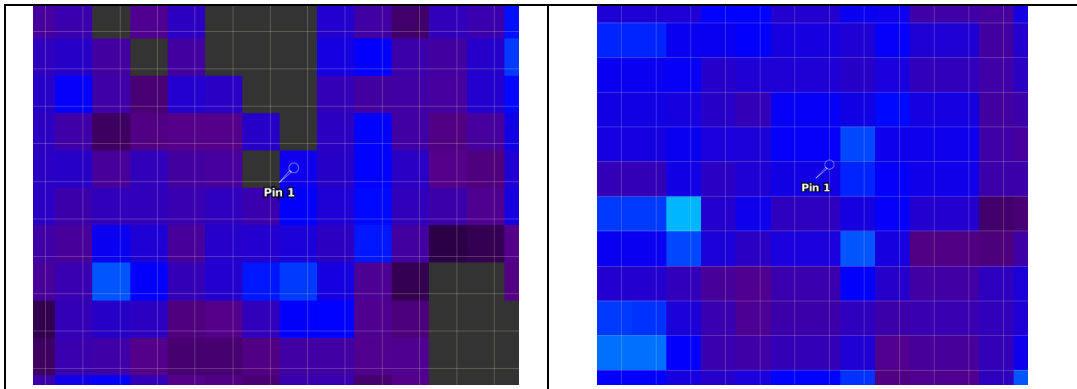


Figure 38: ITTra, OGVI on 20170702 (left) and 20170703 (right)

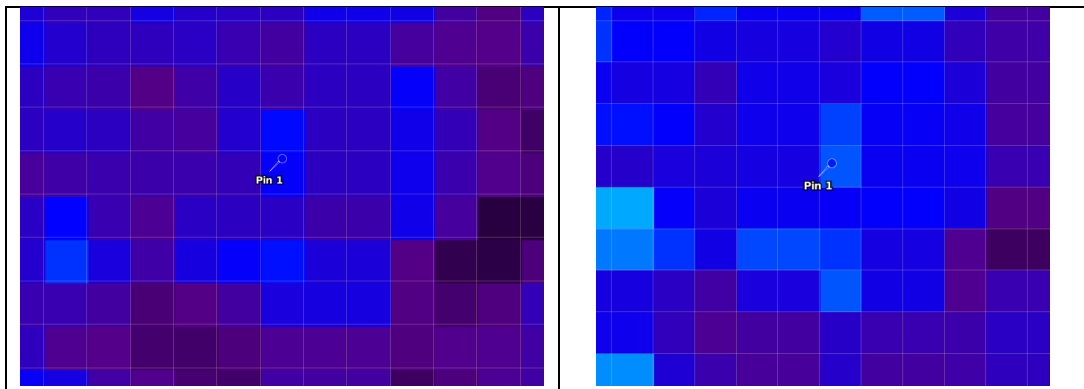


Figure 39: ITTra, OGVI on 20170706 (left) and 20170707 (right)

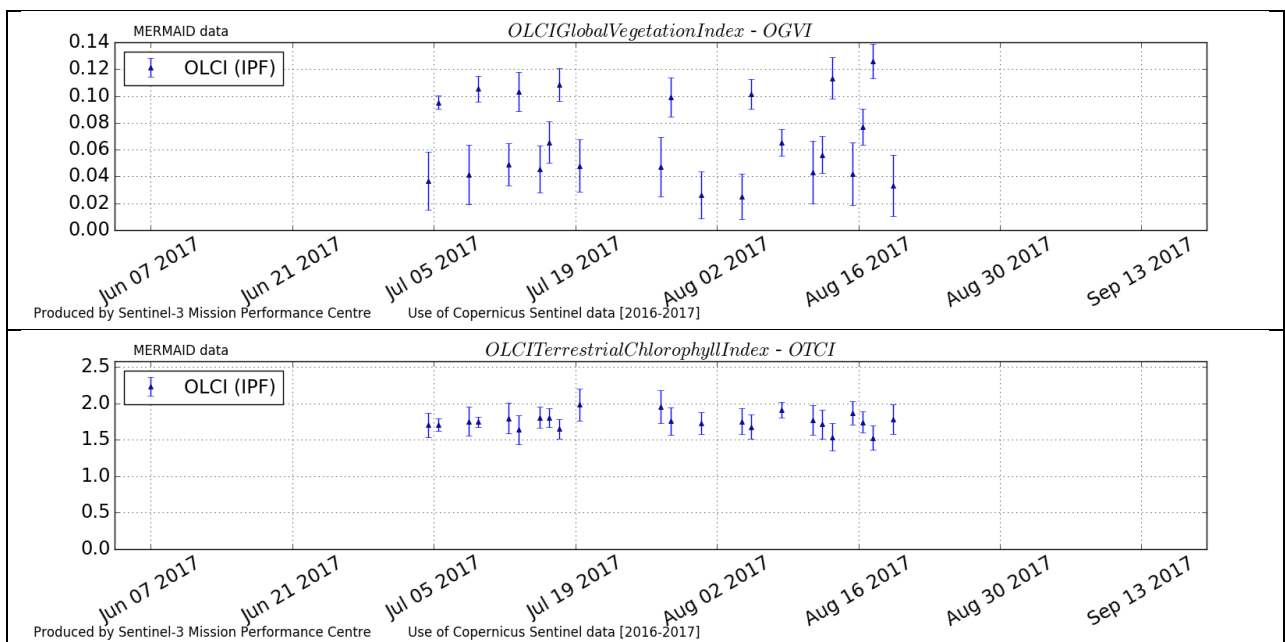


Figure 40: SPAl time series



Sentinel-3 MPC
S3-A OLCI Cyclic Performance Report
Cycle No. 021

Ref.: S3MPC.ACR.PR.01-021
 Issue: 1.0
 Date: 08/09/2017
 Page: 36

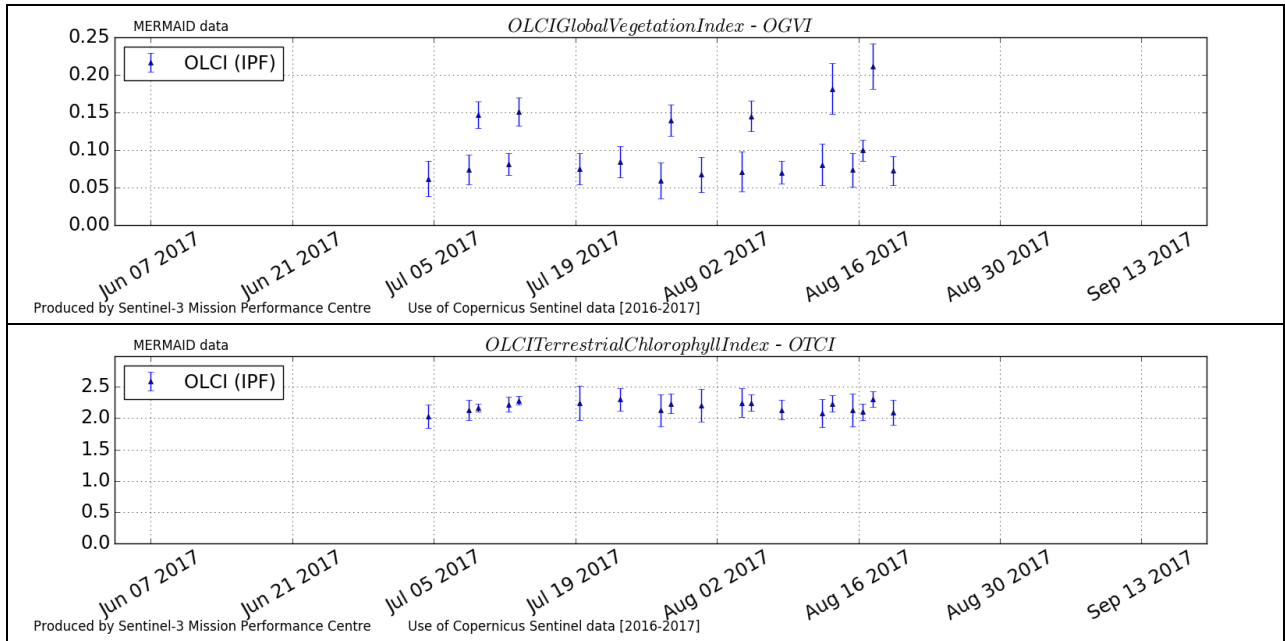


Figure 41: SPVal time series

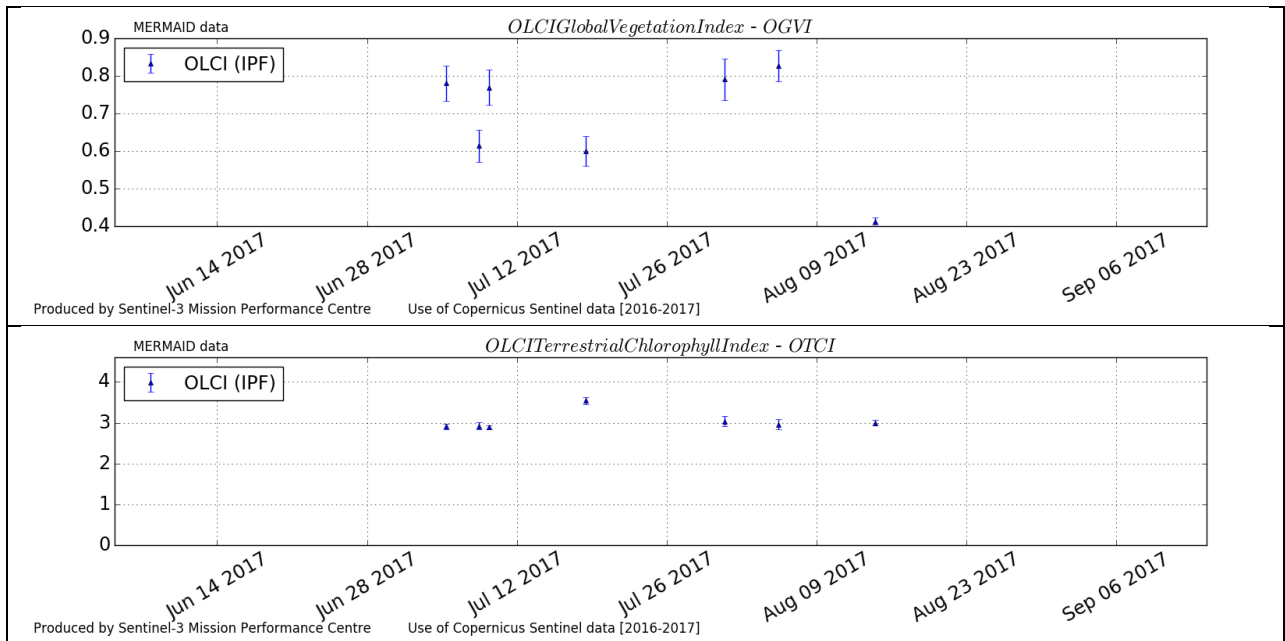


Figure 42: UKNfo time series



Sentinel-3 MPC
S3-A OLCI Cyclic Performance Report
Cycle No. 021

Ref.: S3MPC.ACR.PR.01-021
 Issue: 1.0
 Date: 08/09/2017
 Page: 37

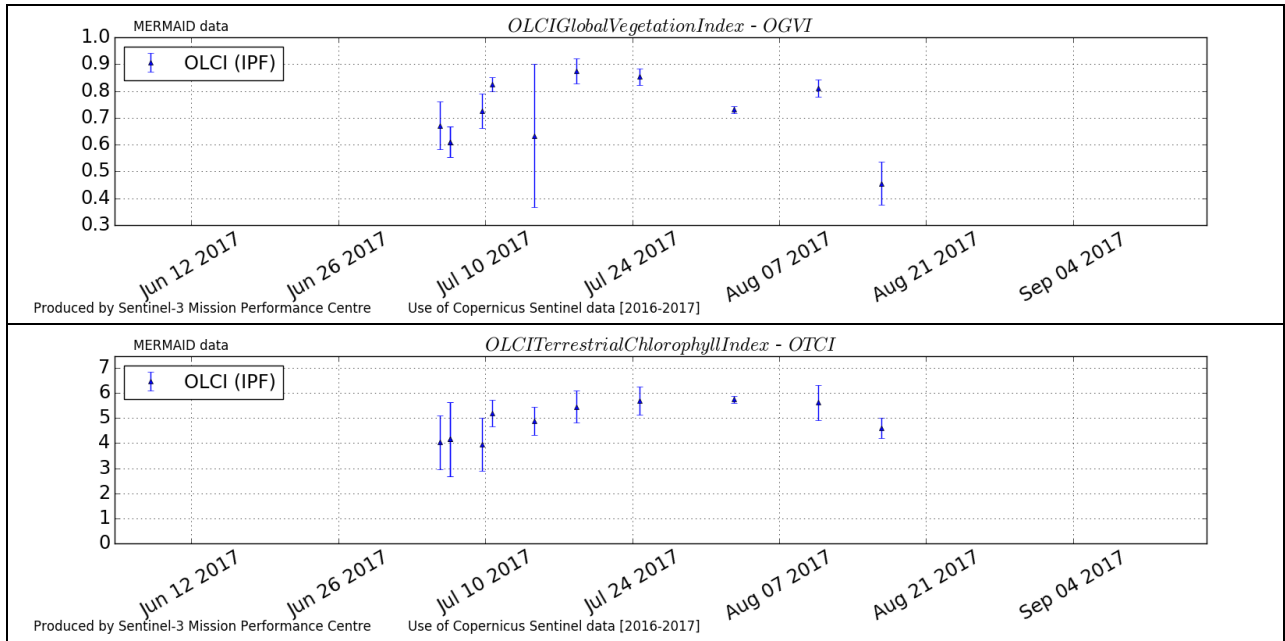


Figure 43: USNe1 time series

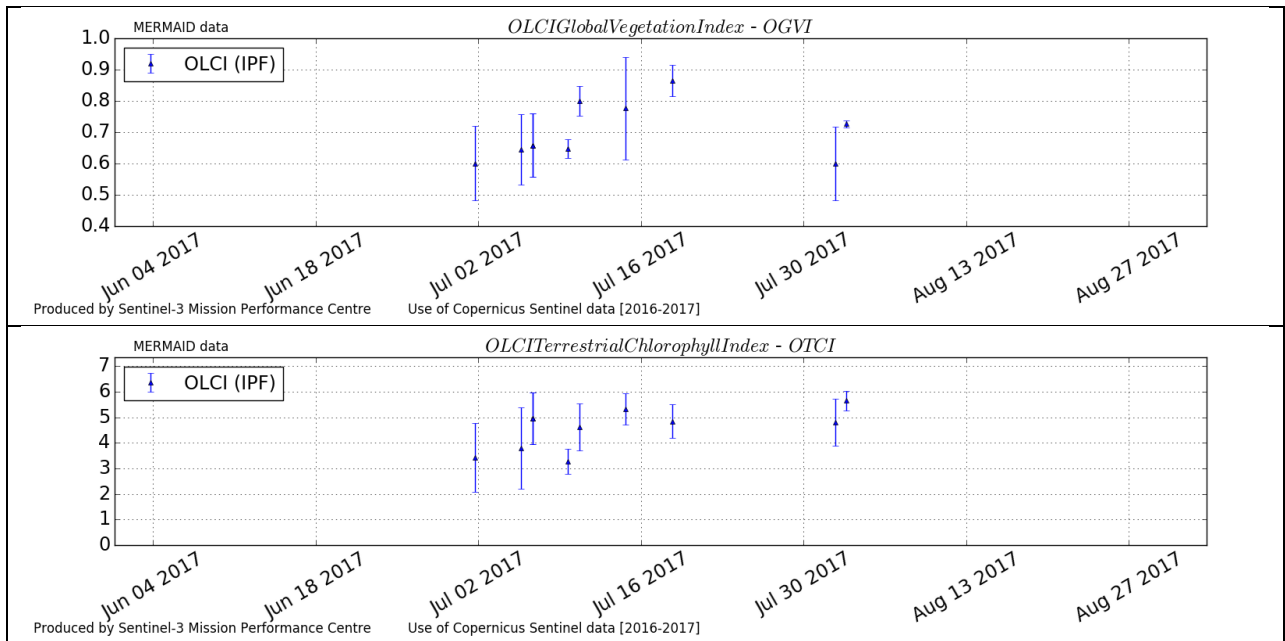


Figure 44: USNe2 time series



Sentinel-3 MPC
S3-A OLCI Cyclic Performance Report
Cycle No. 021

Ref.: S3MPC.ACR.PR.01-021
 Issue: 1.0
 Date: 08/09/2017
 Page: 38

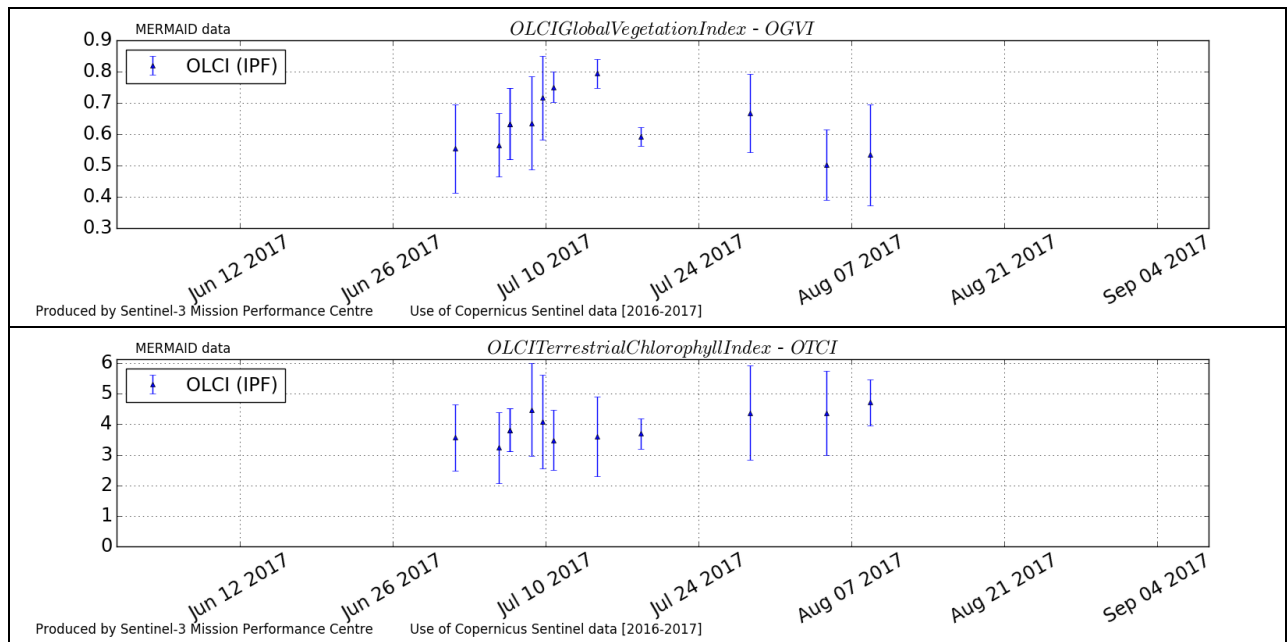


Figure 45: USNe3 time series

3.2 [OLCI-L2LRF-CV-410 & OLCI-L2LRF-CV-420] – Cloud Masking & Surface Classification for Land Products

There has been no update on Cloud Masking & Surface Classification for Land t during the cycle. Last figures (cycle 20) are considered valid.

3.3 Validation of Integrated Water Vapour over Land

There has been no update on Integrated Water Vapour over Land validation quantitative assessment during the cycle. Last figures (cycle 15) are considered valid.

Qualitative assessment by product inspection showed no detectable performance evolution.

	Sentinel-3 MPC S3-A OLCI Cyclic Performance Report Cycle No. 021	Ref.: S3MPC.ACR.PR.01-021 Issue: 1.0 Date: 08/09/2017 Page: 39
--	---	---

4 Level 2 Water products validation

4.1 [OLCI-L2-CV-210, OLCI-L2-CV-220] – Vicarious calibration of the NIR and VIS bands

There has been no update on SVC (System Vicarious Calibration) during Cycle 021.

4.2 [OLCI-L2WLR-CV-300, OLCI-L2WLR-CV-310, OLCI-L2WLR-CV-32, OLCI-L2WLR-CV-330, OLCI-L2WLR-CV-340, OLCI-L2WLR-CV-350, OLCI-L2WLR-CV-360 and OLCI-L2WLR-CV-370] – Level 2 Water-leaving Reflectance product validation.

Activities done

- ❖ The focus for this time period has been on the Near Real Time data.
- ❖ All extractions and statistics have been regenerated for the last three months (July 1st 2017 onward; rolling archive limitation). The available matchups therefore cover the summer situation. Time range available for last processing period covered April 30th to July 1st.
- ❖ A MPMF data provision failure has been reported. The amount of available data is therefore limited
- ❖ MOBY and AERONET-OC in-situ data are available for this time period. However no OLCI data are available over MOBY for this reporting period. In addition, AAOT AERONET-OC station is being fully refurbished. No data are therefore available on this period either. BOUSSOLE data have been updated but unfortunately do not cover the current period.

Overall Water-leaving Reflectance performance

Figure 46 below presents the scatterplots with statistics of OLCI FR versus in situ reflectance computed for the NRT dataset. The data considered correspond to the latest processing baseline ie including SVC. Table 3 to Table 7 below summarises the statistics over the previous period. The statistics of the current NRT period are presented in Table 8. The lack of OLCI data does not allow drawing definite conclusion but data quality seems in line with expectation.



Sentinel-3 MPC
S3-A OLCI Cyclic Performance Report
Cycle No. 021

Ref.: S3MPC.ACR.PR.01-021
 Issue: 1.0
 Date: 08/09/2017
 Page: 40

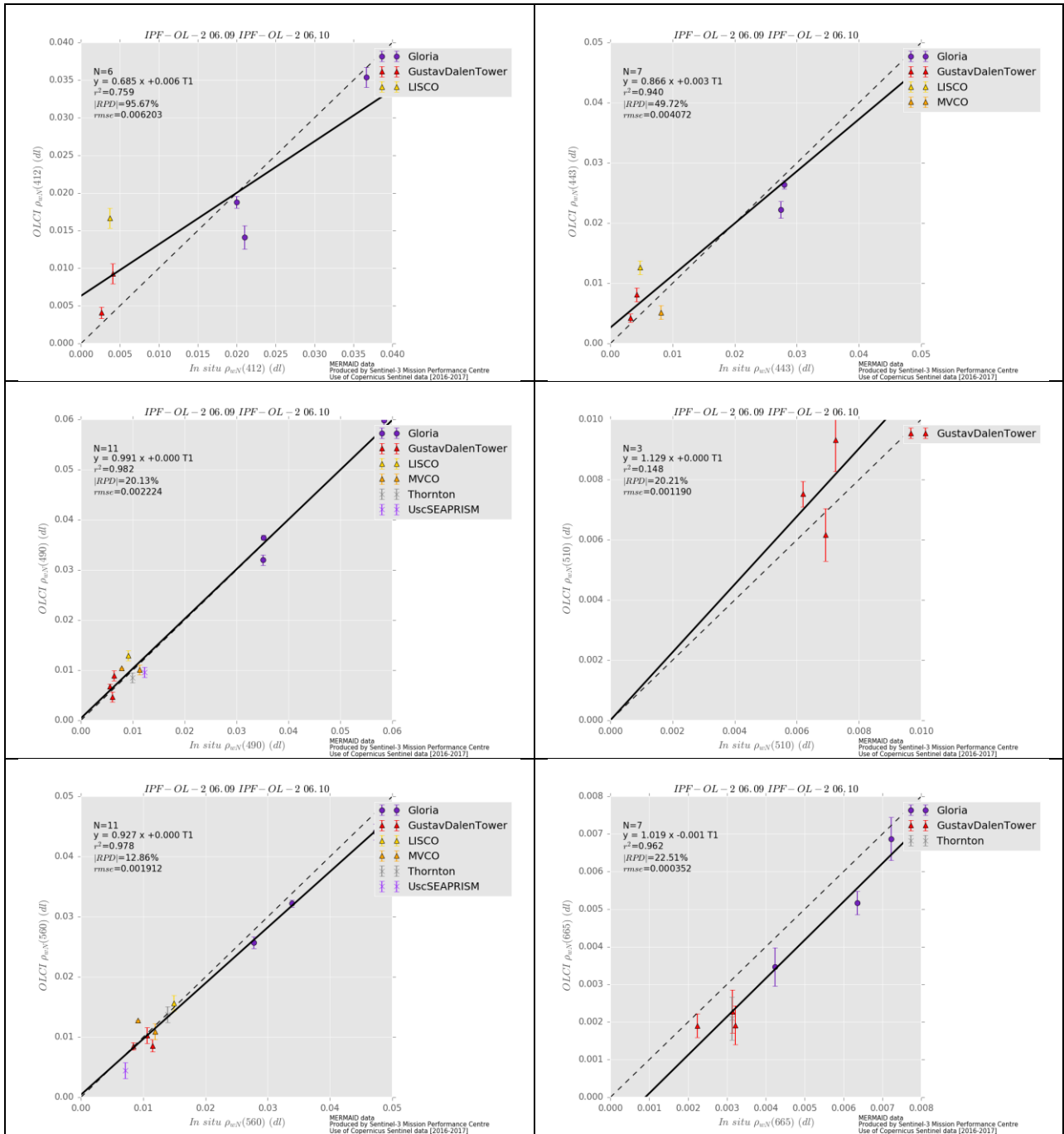


Figure 46: Scatter plots of OLCI versus in situ radiometry (FR data)



Sentinel-3 MPC

S3-A OLCI Cyclic Performance Report

Cycle No. 021

Ref.: S3MPC.ACR.PR.01-021

Issue: 1.0

Date: 08/09/2017

Page: 41

Table 3: FR statistics over December 2016-March 2017 reporting period

lambda	N	RPD	RPD	MAD	RMSE	slope	int.	r2
412	25	70,55%	77,47%	0,0055	0,0071	0,9486	0,0061	0,6787
443	25	43,34%	44,27%	0,0045	0,0056	1,1251	0,0028	0,9037
490	24	28,53%	28,53%	0,0048	0,0059	1,1634	0,0016	0,9611
510	2	31,69%	31,69%	0,0091	0,0093	2,0459	-0,0207	1,0000
560	17	15,44%	16,95%	0,0037	0,0052	1,1350	0,0003	0,9655
665	25	10,56%	34,24%	0,0010	0,0032	1,3661	-0,0013	0,9236

Table 4: FR statistics over February 2017-April 2017 reporting period

lambda	N	RPD	RPD	MAD	RMSE	slope	int.	r2
412	60	88.15%	93.77%	0.0052	0.0066	1.0404	0.0048	0.6176
443	60	46.70%	50.43%	0.0038	0.0049	1.1195	0.0026	0.8046
490	59	31.38%	32.56%	0.0039	0.0046	1.1397	0.0019	0.9263
510	19	27.06%	27.06%	0.0050	0.0055	1.1474	0.0021	0.9486
560	53	13.42%	16.58%	0.0024	0.0035	1.1281	0.0001	0.9379
665	51	1.02%	29.79%	0.0000	0.0012	1.0202	-0.0001	0.7892

Table 5 FR statistics over April 2017-June 2017 reporting period

lambda	N	RPD	RPD	MAD	RMSE	slope	intercept	r2
400	2	17.9%	17.9%	0.0088	0.0100	-2.3992	0.1784	1.0000
412	15	66.3%	66.3%	0.0055	0.0062	1.0618	0.0046	0.9611
443	15	36.7%	37.0%	0.0037	0.0044	1.1107	0.0023	0.9454
490	20	32.1%	32.3%	0.0038	0.0044	1.0153	0.0036	0.8224
510	10	35.9%	35.9%	0.0045	0.0048	0.8626	0.0064	0.7505
560	21	17.0%	21.9%	0.0020	0.0034	1.0925	0.0006	0.9205

Table 6: FR statistics over May 1st to July 10th reporting period

lambda	N	RPD	RPD	MAD	RMSE	slope	intercept	r2
412	35	30.5%	38.2%	0.0025	0.0060	0.9699	0.0033	0.9364
443	43	25.2%	32.9%	0.0023	0.0061	1.0444	0.0012	0.9546
490	52	15.2%	22.2%	0.0020	0.0055	1.0462	0.0007	0.9756
510	21	24.1%	24.9%	0.0026	0.0039	1.1577	0.0004	0.9946
560	52	2.4%	11.1%	0.0004	0.0045	1.0196	-0.0002	0.9701
665	32	-6.9%	17.7%	-0.0002	0.0023	0.9830	-0.0001	0.8423

Table 7: FR statistics over the current reporting period (July 11th to August 23rd)

lambda	N	RPD	RPD	MAD	RMSE	slope	intercept	r2
412	19	18.0%	32.2%	0.0008	0.0066	1.0075	0.0006	0.9346
443	24	10.2%	24.1%	0.0012	0.0072	1.0752	-0.0012	0.9524
490	32	8.0%	18.8%	0.0012	0.0062	1.0504	-0.0005	0.9743
510	10	17.6%	19.3%	0.0011	0.0014	0.9560	0.0014	0.6316
560	32	-1.0%	13.0%	-0.0002	0.0055	1.0179	-0.0008	0.9618
665	22	-10.8%	18.4%	-0.0004	0.0027	0.9028	0.0003	0.7552

Table 8: FR Statistics over the current reporting period (July 1st to September 7th)

lambda	N	RPD	RPD	MAD	RMSE	slope	intercept	r2
412	6	81.5%	95.7%	0.0017	0.0064	0.6848	0.0063	0.7589
443	7	31.6%	49.7%	0.0003	0.0041	0.8661	0.0026	0.9401
490	11	5.8%	20.1%	0.0003	0.0022	0.9909	0.0004	0.9818
510	3	13.0%	20.2%	0.0009	0.0015	1.1289	0.0000	0.1477
560	11	-4.5%	12.9%	-0.0009	0.0021	0.9270	0.0004	0.9784
665	7	-22.5%	22.5%	-0.0008	0.0009	1.0191	-0.0009	0.9618

Figure 48 and 40 below shows the time series of available AERONET-OC stations from april onward at 490nm waveband. Again the lack of either OLCI or in situ data on the current period does not allow drawing definite conclusion. For the few stations with in situ and satellite data, the results appear nonetheless nominal.

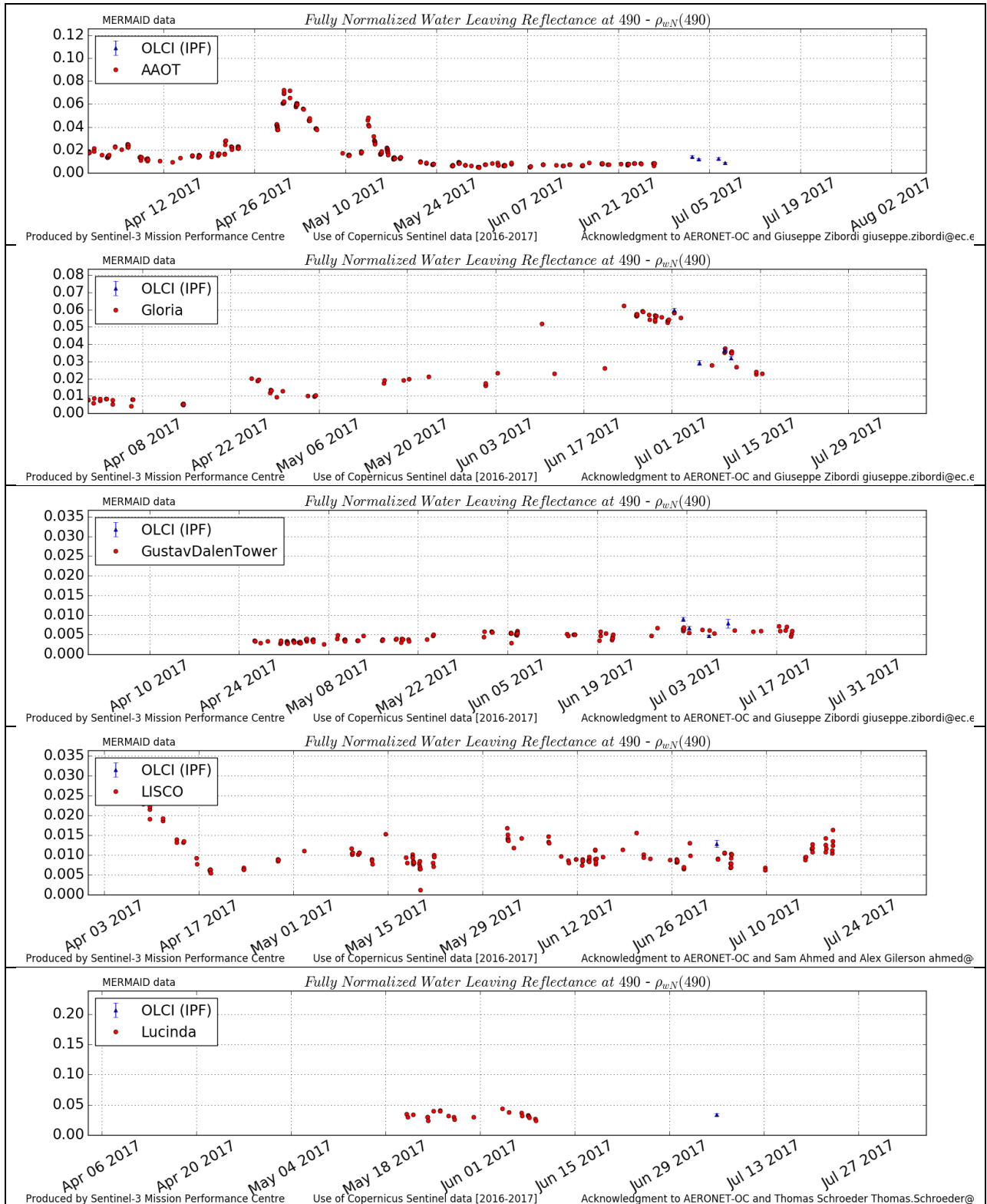


Figure 47: OLCI and AERONET-OC radiometric time series at 490nm.



Sentinel-3 MPC

S3-A OLCI Cyclic Performance Report

Cycle No. 021

Ref.: S3MPC.ACR.PR.01-021
 Issue: 1.0
 Date: 08/09/2017
 Page: 44

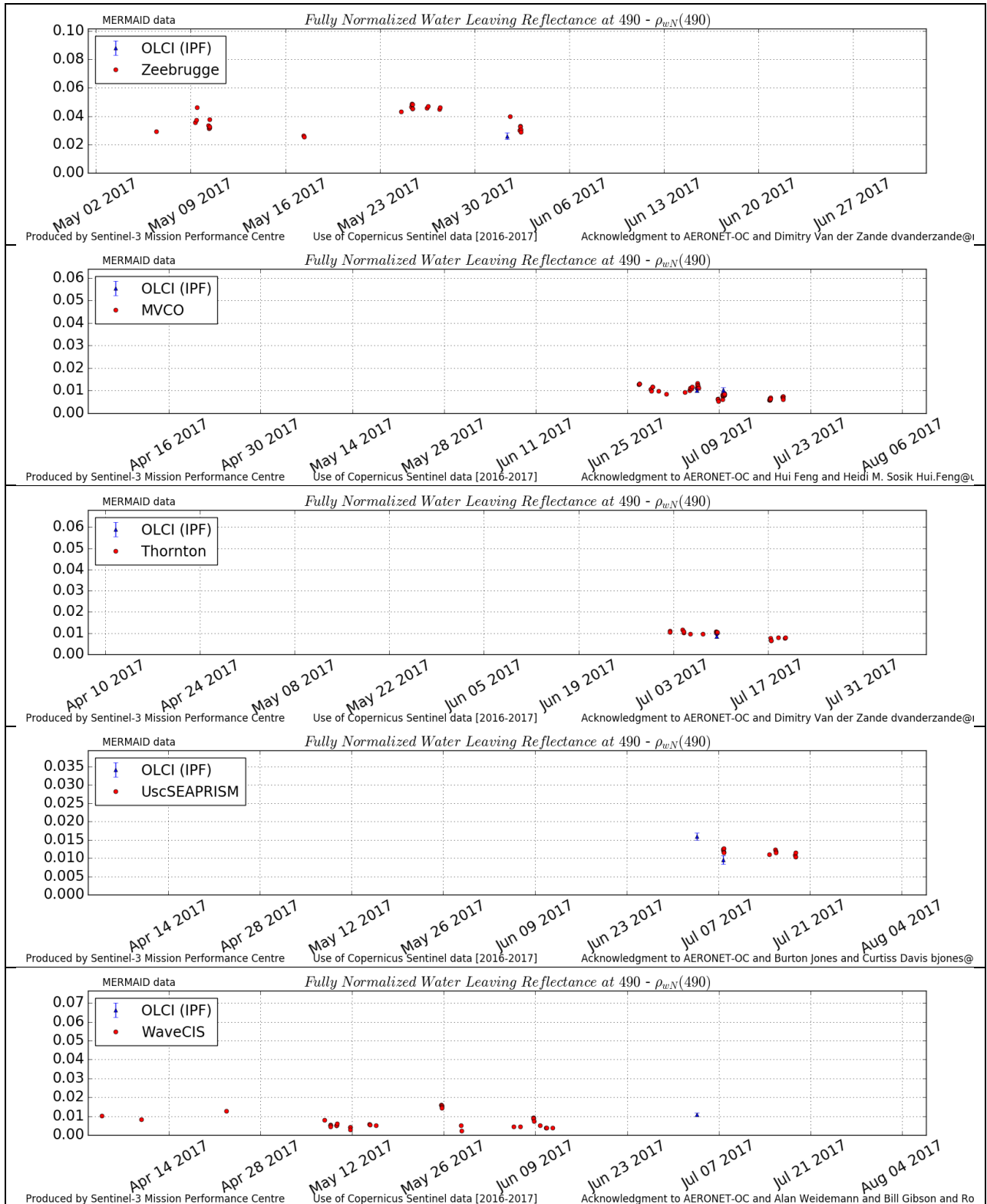


Figure 48: OLCI and AERONET-OC radiometric time series at 490nm.

	Sentinel-3 MPC S3-A OLCI Cyclic Performance Report Cycle No. 021	Ref.: S3MPC.ACR.PR.01-021 Issue: 1.0 Date: 08/09/2017 Page: 45
--	---	---

4.3 [OLCI-L2WLR-CV530] Validation of Aerosol Product

There has been no update on Aerosol Products validation quantitative assessment during the cycle. Last figures (cycle 18) are considered valid.

Qualitative assessment by product inspection showed no detectable performance evolution.

	<p>Sentinel-3 MPC</p> <p>S3-A OLCI Cyclic Performance Report</p> <p>Cycle No. 021</p>	<p>Ref.: S3MPC.ACR.PR.01-021</p> <p>Issue: 1.0</p> <p>Date: 08/09/2017</p> <p>Page: 46</p>
--	--	--

5 Level 2 SYN products validation

5.1 [SYN-L2-CV-100]

Following latest corrections and improvement included in SYNERGY L2 processing chains (related to the handling of cloud masks, to the aerosol interpolation ...), the quality assessment of the SYNERGY Level 2 products have been investigated by S3MPC ESLs.

The current SYN L2 products show an over-estimation of the Aerosol Optical Thickness and, as consequences, an over-correction of smallest spectral wavebands (first line of Figure 51) and higher surface reflectance, especially in oblique view (last panel of Figure 51).

This over-estimation is mainly present over clear area with values higher than expected (around 1.9 over Central Europe or Northern America). However, the Aerosol Optical Thickness computed at 550 nm provide expected values (around 0,4) close to cloudy areas (Figure 50 – the cloud mask is represented by grey pixels).



**Figure 49 : OLCI RGB image from
S3A_OL_1_EFR____20170619T101637_20170619T101937_20170619T122047_0179_019_065_2160_SVL_O_NR_
002.SEN3**

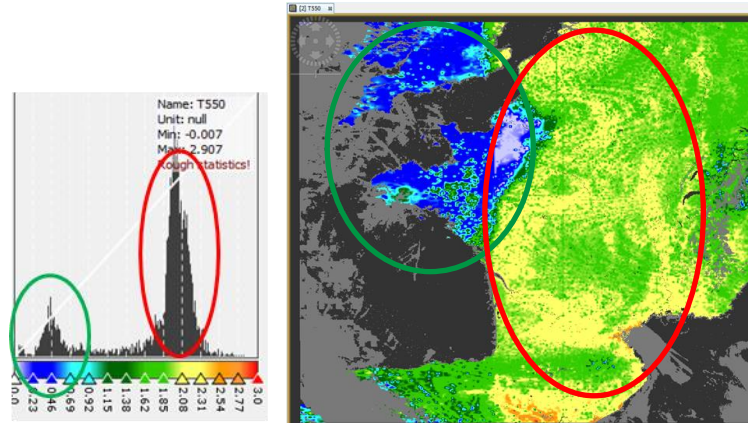


Figure 50 : Maps and histogram of AOT@550 nm from associated SYN product;
S3A_SY_2_SYN____20170619T101637_20170619T101937_20170621T033649_0179_019_065_2160_LN2_O_NT_002.SEN3

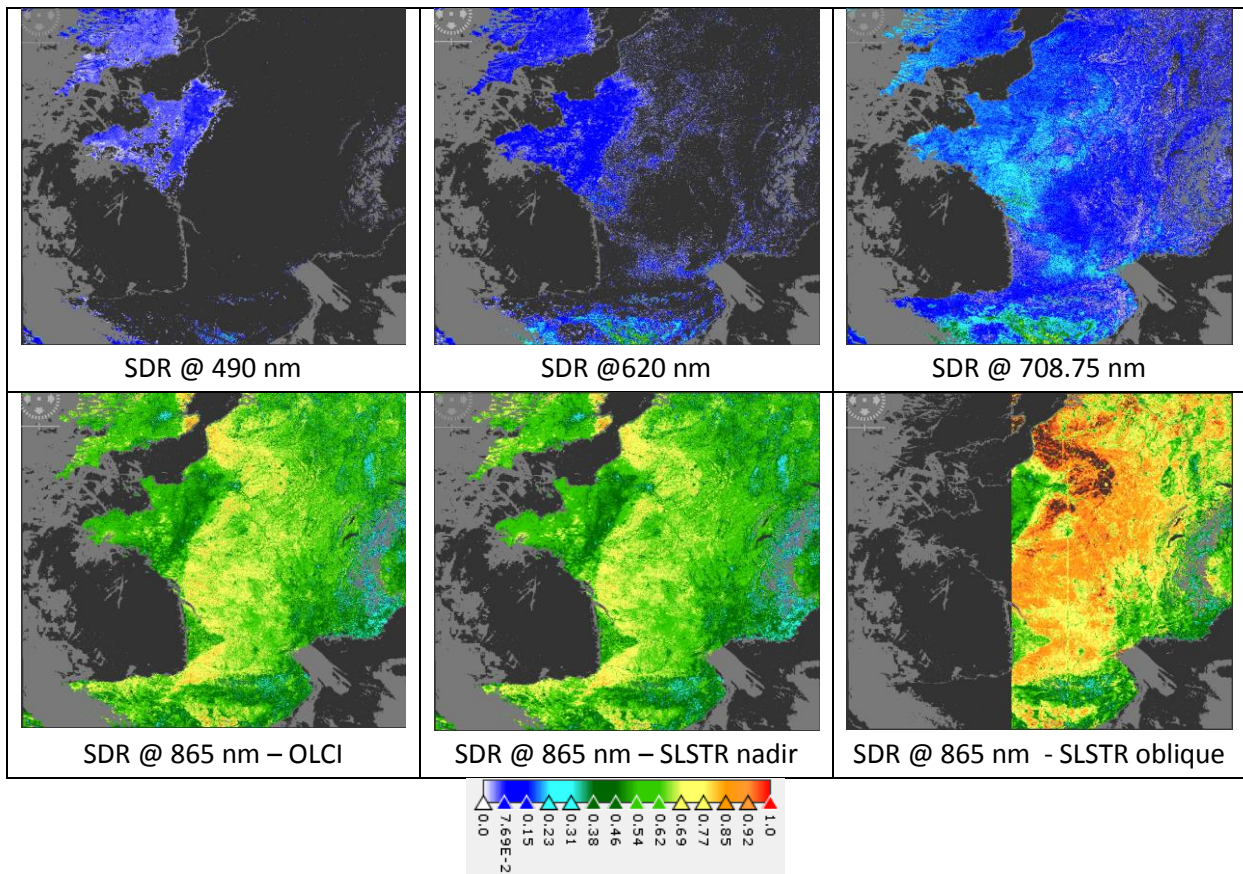


Figure 51 : Surface directional Reflectance associated with different OLCI and SLSTR channels from
S3A_SY_2_SYN____20170619T101637_20170619T101937_20170621T033649_0179_019_065_2160_LN2_O_NT_002.SEN3. The unfilled land pixels are the one associated with a negative surface directional reflectance

To understand and correct this behavior, we investigate jointly the performance of the S3 SYNERGY Aerosol retrieval (to understand the impact of the angular and spectral constraints) and the impact of the different SYNERGY channels on the aerosol retrieval.

All tests are performed over Australia acquired in February 2017 (Figure 52) and the analyzed results are the one directly produced by the aerosol retrieval section (i.e. without performing any cosmetic filling or smoothing)

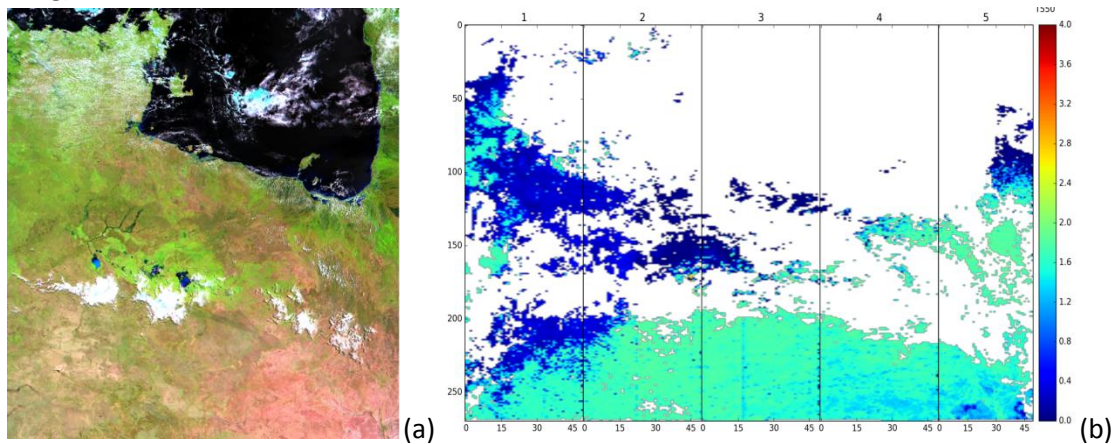


Figure 52 : (a) RGB image of the SLSTR Nadir view and (b) SYN L2 Aerosol Optical Thickness obtained with current SYN L2 IPF from S3A_SL_1_RBT____20170227T003224_20170227T003524_20170329T135202_0180_015_002_____LR1_D_NT_001.SEN3

First, strange behaviors have been observed on the surface directional reflectance associated with the SLSTR S4 channel (1.375 μm) in both views (figure X). These patterns are directly transferred from the inputs SLSTR L1B products, including very low radiances and a “pixelated” patterns.

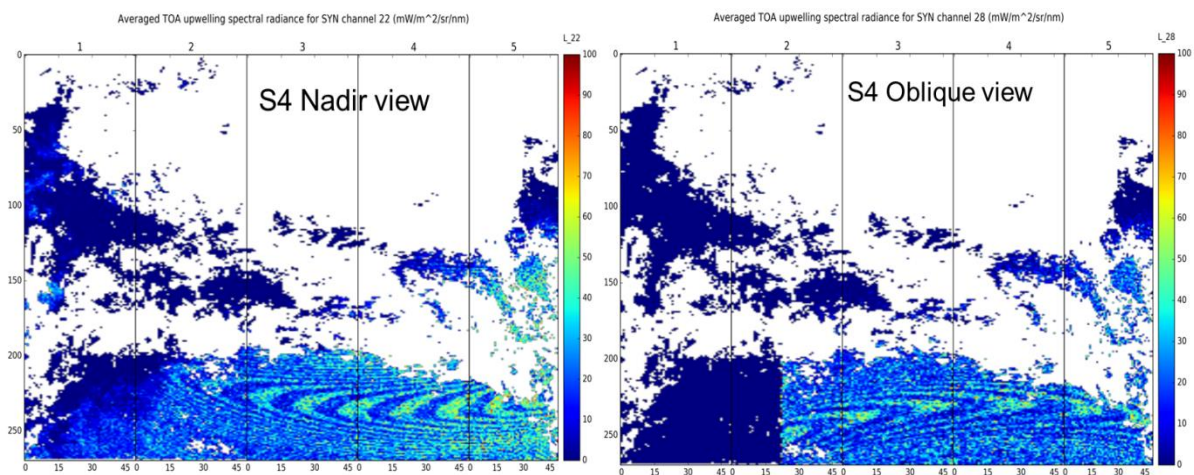
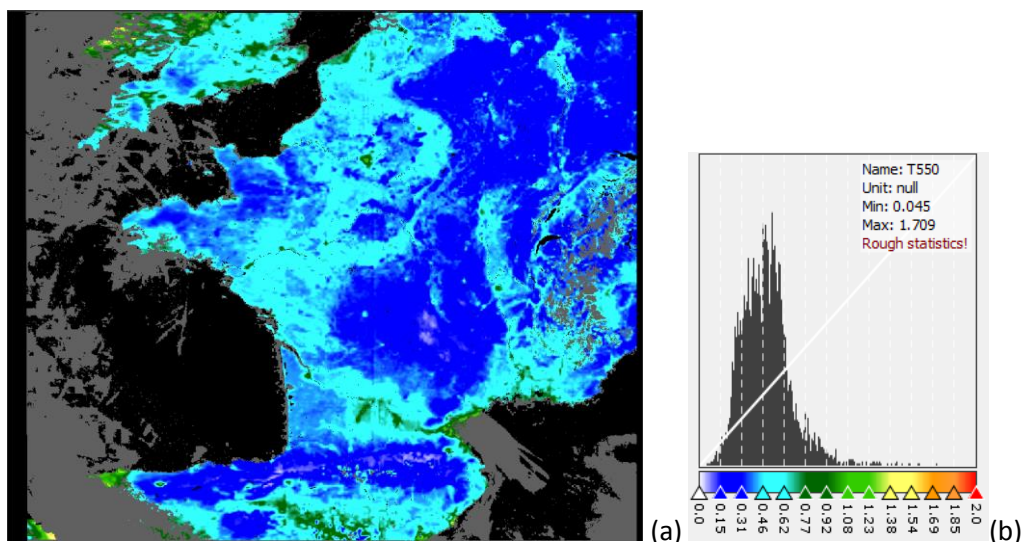


Figure 53 : TOA radiances associated with SLSTR S4 channel and used in the SYN L2 Aerosol retrieval

After iterations with SLSTR ESLs, it has been confirmed that the S4 channel is only dedicated to the cirrus detection and low radiances are “normal” behavior in case of clear sky images. As consequences, **this channel should not be used inside SYN L2 aerosol retrieval section and a Change Request is currently under preparation to include this evolution in SYN L2 IPF.**

If the SLSTR S4 channel is not taken into account in the SYN L2 aerosol retrieval section, the outputted values of Aerosol Optical thickness at 550 nm are closer to the expected one as show in Figure 54 for the European scene. The impact of this evolution is also well observed on surface reflectances with consistent outputs for the different OLCI and SLSTR channels (Figure 55).



**Figure 54 : Maps and histogram of AOT@550 nm from SYN product;
S3A_SY_2_SYN____20170619T101637_20170619T101937_REPROCESSED without SLSTR S4 taken into account in
the aerosol retrieval**



Sentinel-3 MPC
S3-A OLCI Cyclic Performance Report
Cycle No. 021

Ref.: S3MPC.ACR.PR.01-021
 Issue: 1.0
 Date: 08/09/2017
 Page: 50

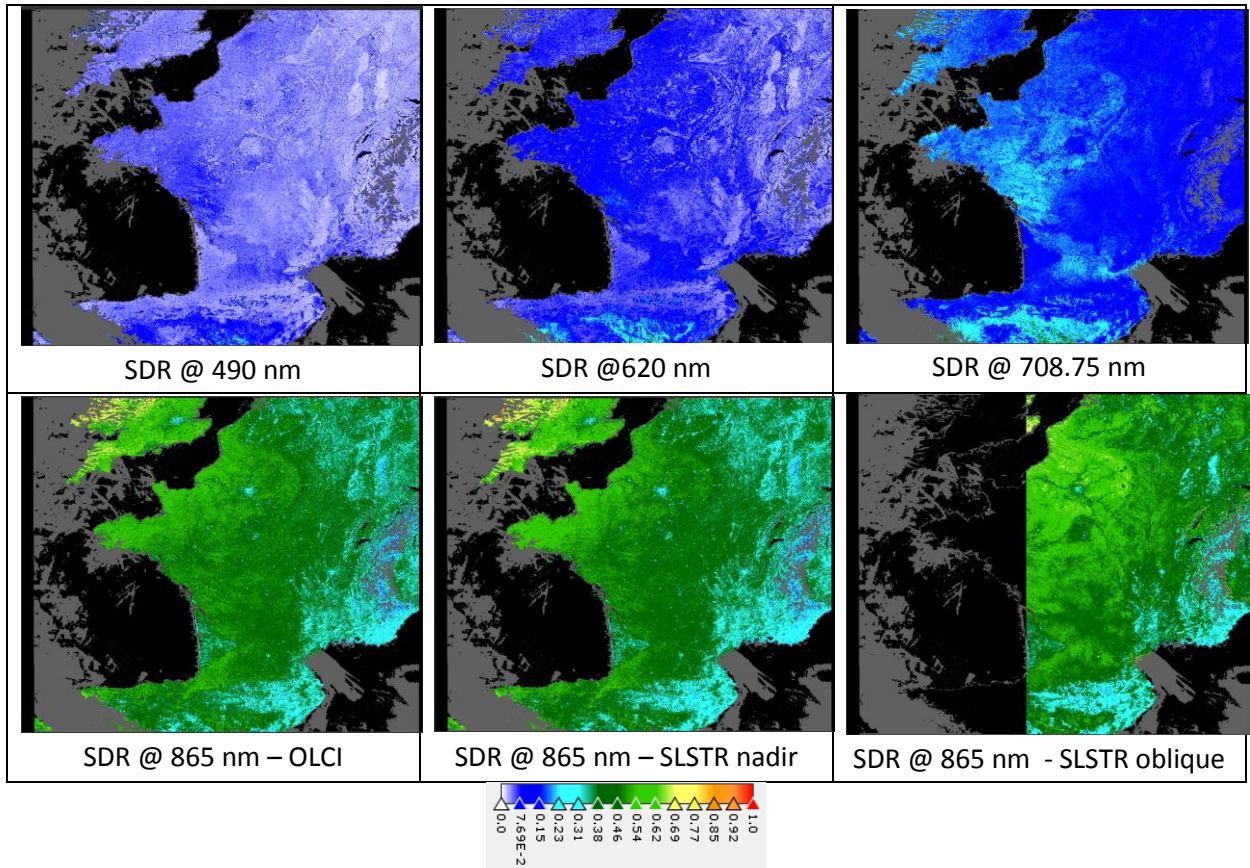


Figure 55 : Surface directional Reflectance associated with different OLCI and SLSTR channels from S3A_SY_2_SYN___20170619T101637_20170619T101937_REPROCESSED without SLSTR S4 channel taken into account in the aerosol retrieval section

Once this evolution included in the development branch of the IPF, the performance of the aerosol retrieval section has been investigated with regards to the impact of spectral and angular constraints. The influence of NDVI values has also been taken as reference to understand the behavior of this section:

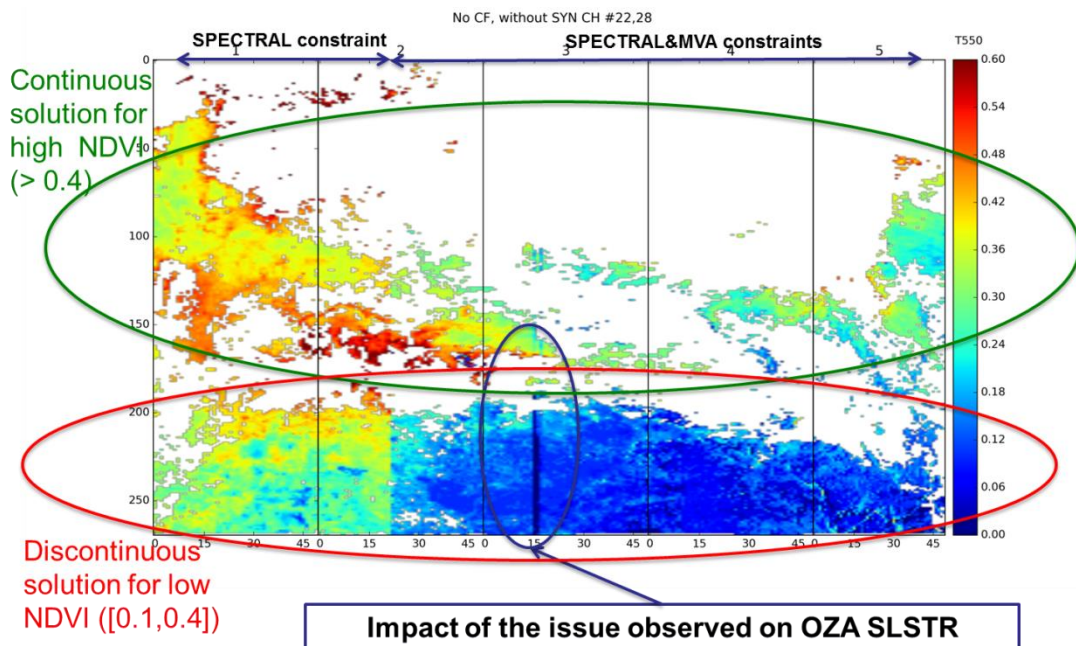
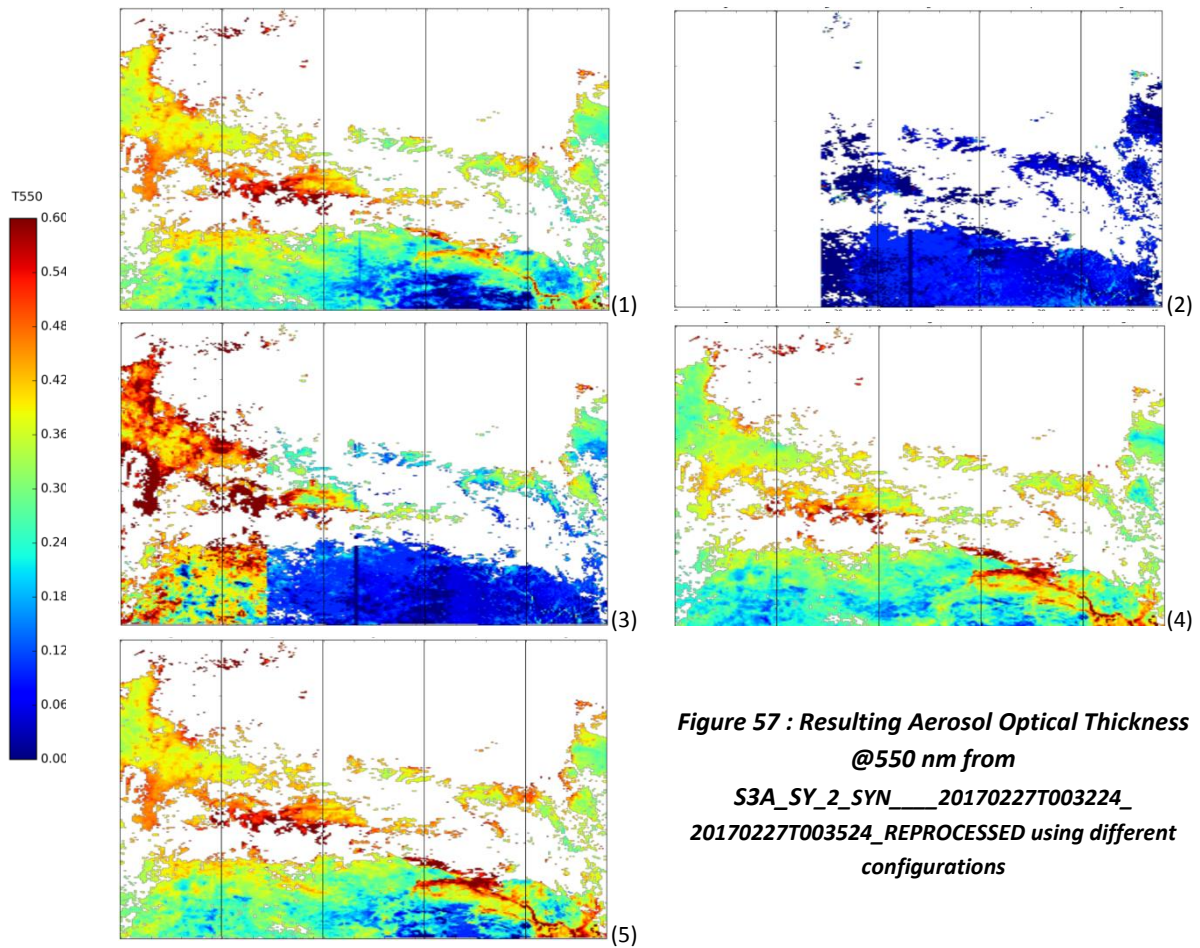


Figure 56 : Analysis of the Aerosol retrieval outputs from S3A_SY_2_SYN____20170227T003224_20170227T003524_REPROCESSED

Different configurations for Aerosol retrieval section have been then tested and the resulting SYN L2 Aerosol Optical thickness has been analyzed (see Figure 56). Note that in each scenario, SLSTR S4 channels are no longer taken into account.

1. Using spectral constraint only
2. Using Angular constraint only
3. Using only SLSTR channels
4. Using only OLCI channels
5. Using only OLCI and SLSTR nadir view channels



This investigation is still on-going but the first results show un-correlated solutions between the angular and the spectral constraints (see third panel on Figure 57). In particular, it has been underlined that the angles associated with oblique view are very different from the one associated with OLCI and SLSTR nadir view (Figure 58). This difference could explain inconsistencies in the aerosol retrieval.

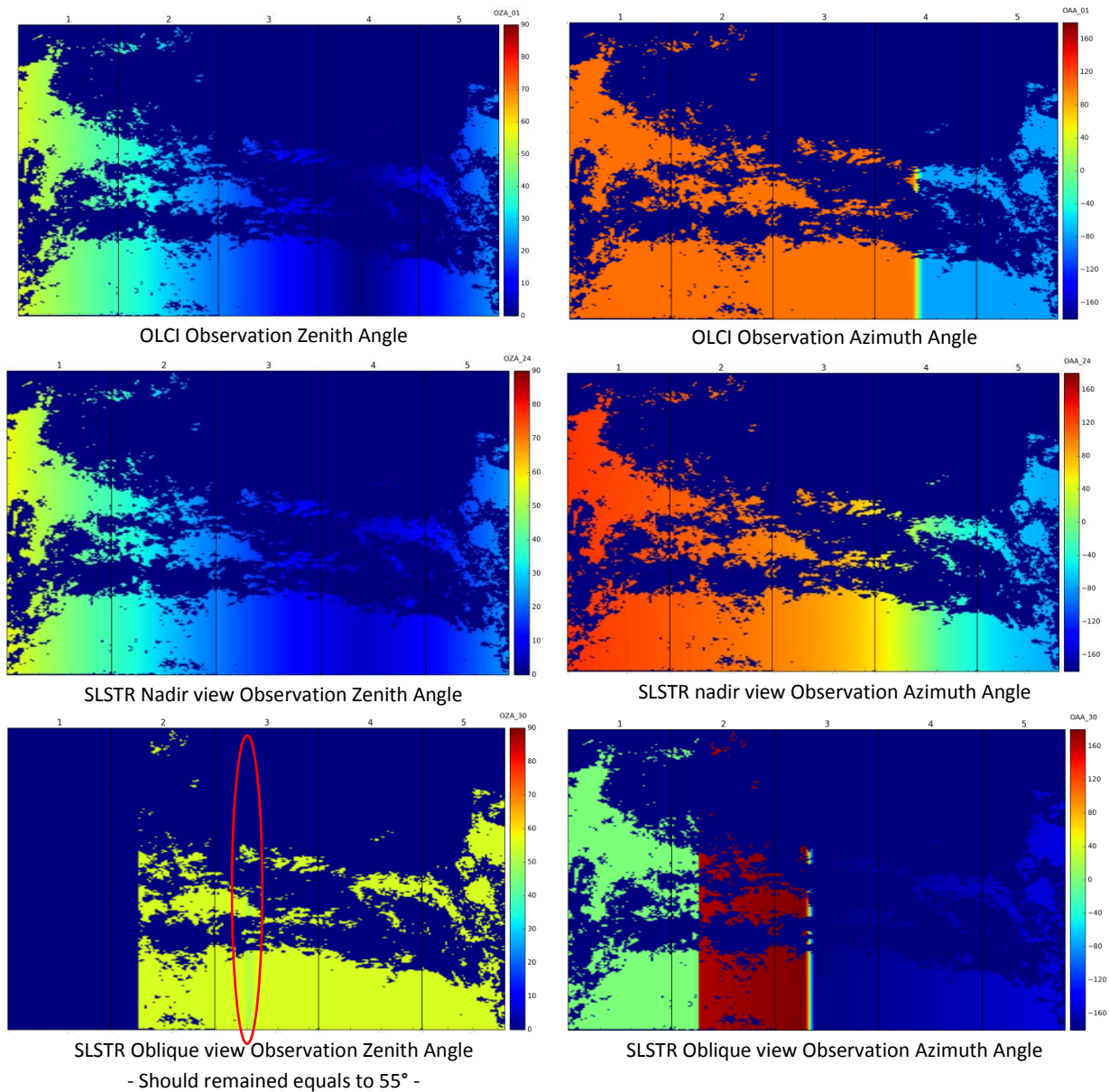


Figure 58 : Observation angles associated with each contribution of SYN L2 aerosol retrieval section

An issue regarding the Observation Zenith Angles internally associated with SLSTR oblique view has been raised and is currently under investigation (see last line – left panel on Figure 58). This issue, linked to a wrong interpolation inside SYN IPF, creates strong vertical inconsistent line in the SYN L2 product, observed on Figure 56

All these results are still under investigations but confirm the required evolution of SYN L2 processing chains excluding any channel dedicated to aerosol absorption or cloud detection.

	Sentinel-3 MPC S3-A OLCI Cyclic Performance Report Cycle No. 021	Ref.: S3MPC.ACR.PR.01-021 Issue: 1.0 Date: 08/09/2017 Page: 54
--	---	---

6 Events

Two OLCI Radiometric Calibration Sequences have been acquired during Cycle 021:

- ❖ S04 sequence (diffuser 1) on 22/07/2017 08:09 to 08:11 (absolute orbit 7437)
- ❖ S05 sequence (diffuser 2) on 22/07/2017 09:50 to 09:52 (absolute orbit 7438)

	Sentinel-3 MPC S3-A OLCI Cyclic Performance Report Cycle No. 021	Ref.: S3MPC.ACR.PR.01-021 Issue: 1.0 Date: 08/09/2017 Page: 55
--	---	---

7 Appendix A

Other reports related to the Optical mission are:

- ❖ S3-A SLSTR Cyclic Performance Report, Cycle No. 021 (ref. S3MPC.RAL.PR.02-021)

All Cyclic Performance Reports are available on MPC pages in Sentinel Online website, at:
<https://sentinel.esa.int>

End of document